

~~CONFIDENTIAL~~

NACA RM L58G17



RESEARCH MEMORANDUM

UNCLASSIFIED
*Research Abstract (RA) # 8-14-58
skm 8-15-88*

THEORETICAL CALCULATIONS OF THE STABILITY DERIVATIVES
AT SUPERSONIC SPEEDS FOR A HIGH-SPEED
AIRPLANE CONFIGURATION

By Kenneth Margolis and Percy J. Bobbitt

Langley Aeronautical Laboratory
Langley Field, Va.

LIBRARY COPY

LANGLEY RESEARCH CENTER
LIBRARY, NASA
HAMPTON, VIRGINIA

CLASSIFIED DOCUMENT

This material contains information affecting the National Defense of the United States within the meaning of the espionage laws, Title 18, U.S.C., Secs. 793 and 794, the transmission or revelation of which in any manner to an unauthorized person is prohibited by law.

NATIONAL ADVISORY COMMITTEE FOR AERONAUTICS

WASHINGTON
October 8, 1953

~~CONFIDENTIAL~~

UNCLASSIFIED



NACA RM L53G17

~~CONFIDENTIAL~~

3 1176 01437 1299

NATIONAL ADVISORY COMMITTEE FOR AERONAUTICS

RESEARCH MEMORANDUM

THEORETICAL CALCULATIONS OF THE STABILITY DERIVATIVES

AT SUPERSONIC SPEEDS FOR A HIGH-SPEED

AIRPLANE CONFIGURATION

By Kenneth Margolis and Percy J. Bobbitt

SUMMARY

Theoretical calculations of the stability derivatives at supersonic speeds for a high-speed airplane configuration are presented. The range of Mach numbers considered includes those cases for which the wing and tail surfaces have subsonic leading edges, supersonic leading edges, and combinations of the two. The methods of analysis are discussed; these represent detailed consideration of the important effects and contributions of the various airplane components utilizing available theories and theoretically justifiable and reasonable approximations.

Results of the investigation, which are applicable to motions involving small angles of attack and sideslip and low rates of rolling, pitching, and yawing, are presented in the form of graphs illustrating the variation of the stability derivatives with Mach number.

INTRODUCTION

The prediction of the stability of complete airplane and missile configurations requires a knowledge of the aerodynamic forces and moments acting on all component surfaces of the airframe and the rates of change of these forces and moments with respect to the various attitudes, velocities, and accelerations (i.e., stability derivatives). Design of airplanes and missiles for automatic stabilization has accentuated the need for this information while the design is still in its initial stages. Thus the problem of estimating by theoretical means the forces, moments, and resulting stability derivatives of complete airplane configurations at supersonic speeds is one of considerable interest and importance. This is particularly true at the present time in view of the difficulties encountered in determining these quantities experimentally for certain motions. While there is considerable information available for isolated

~~CONFIDENTIAL~~

aircraft components there is relatively little knowledge, either of a theoretical or experimental nature, concerning complete configurations. As a result, it is extremely difficult to estimate with accuracy the performance and stability characteristics of present-day missiles and airplanes.

During the past few years (and at present), considerable research effort has been directed towards the theoretical determination of wing-body and body-tail interference effects and the effects of induced flow on the loading characteristics of the component surfaces of complete configurations. Accurate estimates of these mutual and induced interference effects as well as additional studies related to isolated components and components in combination are required before accurate theoretical estimates of stability derivatives for arbitrary complete configurations can be accomplished.

The present paper results from an investigation which concerned primarily the problems involved in adapting, modifying, and extending the available theories as required in order to estimate reliably the stability derivatives at supersonic speeds for arbitrary complete airplane configurations. For purposes of application, a high-speed interceptor-type aircraft was chosen. It is primarily this phase of the investigation, that is, the estimation of stability derivatives for the specific configuration, which is reported herein. The methods used are described; particularly detailed emphasis is given the case of steady rolling. Results of the analysis are presented in the form of graphs illustrating the variation of the stability derivatives with Mach number.

SYMBOLS

x, y, z	Cartesian coordinates
v, w	perturbation velocities along y and z axes, respectively; negative values for w indicate downwash
p, q, r	angular velocities about x , y , and z axes, respectively
α	angle of attack
$\dot{\alpha}$	rate of change of angle of attack with respect to time
β	angle of sideslip
V	flight velocity

$$B = \sqrt{(\text{Mach number})^2 - 1}$$

ρ density of air

ΔC_p coefficient of pressure difference between upper and lower surfaces, positive in the sense of lift

ϕ velocity potential evaluated on upper surface

Γ circulation, $\frac{V}{2} \int_{\text{L.E.}}^{\text{T.E.}} \Delta C_p dx$

S wing area including portion masked by body

A aspect ratio of wing

b wing span

b_{vt} vertical-tail span

\bar{c} mean aerodynamic chord of wing

l distance between center of gravity and center of pressure of sideslipping vertical tail

A_{vt} aspect ratio of vertical tail

C leading-edge slope of vertical tail

$$K = \frac{BA_{vt}}{BA_{vt} - 2BC}$$

a distance from roll axis to wing-body juncture

x_1, y_1 Cartesian coordinates used in analysis for rolling motion

$$X = x - x_1$$

$$Y = y - y_1$$

i variable index, used in summations and as subscripts

$$X_i = x - x_i$$

$$Y_i = y - y_i$$

$\bar{X}_1, \bar{Y}_1, \bar{z}$	$X_1, Y_1,$ and $z,$ respectively, made nondimensional with respect to wing semispan
m	slope of lifting line (absolute value)
k, k_1, k_2	constants
h_1, h_2	y_1 limits of integration
L	lift
Y	side force
L'	rolling moment
N	yawing moment
M	pitching moment
C_L	lift coefficient, $\frac{L}{\frac{1}{2}\rho V^2 S}$
C_Y	side-force coefficient, $\frac{Y}{\frac{1}{2}\rho V^2 S}$
C_l	rolling-moment coefficient, $\frac{L'}{\frac{1}{2}\rho V^2 S b}$
C_n	yawing-moment coefficient, $\frac{N}{\frac{1}{2}\rho V^2 S b}$
C_m	pitching-moment coefficient, $\frac{M}{\frac{1}{2}\rho V^2 S \bar{c}}$

$$C_{L\alpha} = \left(\frac{\partial C_L}{\partial \alpha} \right)_{\alpha \rightarrow 0}$$

$$C_{m\alpha} = \left(\frac{\partial C_m}{\partial \alpha} \right)_{\alpha \rightarrow 0}$$

$$C_{m\dot{\alpha}} = \left(\frac{\partial C_m}{\partial \frac{\dot{\alpha} \bar{c}}{2V}} \right)_{\dot{\alpha} \rightarrow 0}$$

$$C_{mq} = \left(\frac{\partial C_m}{\partial \frac{q \bar{c}}{2V}} \right)_{q \rightarrow 0}$$

$$C_{Yp} = \left(\frac{\partial C_Y}{\partial \frac{pb}{2V}} \right)_{p \rightarrow 0}$$

$$C_{np} = \left(\frac{\partial C_n}{\partial \frac{pb}{2V}} \right)_{p \rightarrow 0}$$

$$C_{lp} = \left(\frac{\partial C_l}{\partial \frac{pb}{2V}} \right)_{p \rightarrow 0}$$

$$C_{Y\beta} = \left(\frac{\partial C_Y}{\partial \beta} \right)_{\beta \rightarrow 0}$$

$$C_{n\beta} = \left(\frac{\partial C_n}{\partial \beta} \right)_{\beta \rightarrow 0}$$

$$C_{l\beta} = \left(\frac{\partial C_l}{\partial \beta} \right)_{\beta \rightarrow 0}$$

$$C_{Yr} = \left(\frac{\partial C_Y}{\partial \frac{rb}{2V}} \right)_{r \rightarrow 0}$$

$$C_{nr} = \left(\frac{\partial C_n}{\partial \frac{rb}{2V}} \right)_{r \rightarrow 0}$$

$$C_{l_r} = \left(\frac{\partial C_l}{\partial \frac{rb}{2V}} \right)_{r \rightarrow 0}$$

Subscripts:

t tail contribution

t,o tail contribution assuming zero end plate

All angles are measured in radians unless indicated otherwise.

SCOPE

The geometry of the configuration under study is shown in figure 1 and the detailed characteristics of the component surfaces are given in table I. Considered in the analysis are the following motions: constant angle of attack, steady rolling, steady pitching, constant vertical acceleration, constant sideslip, and steady yawing. The following stability derivatives are obtained: C_{l_α} , C_{m_α} , C_{Y_p} , C_{n_p} , C_{l_p} , C_{m_q} , $C_{m_{\dot{\alpha}}}$, C_{Y_β} , C_{n_β} , C_{l_β} , C_{Y_r} , C_{n_r} , and C_{l_r} .

All airframe components are considered rigid; wing and tail surfaces are assumed to have zero thickness. The wing, horizontal tail, and body are at zero geometric angle of attack for all motions other than angle of attack. The analysis is carried out within the framework of the linearized theory, the results being valid for small angles of attack and sideslip and for low rates of rolling, pitching, and yawing. In addition, modifications and assumptions are introduced into the analysis as needed in order to cope with the problems encountered in estimating the derivatives for this particular configuration. Although the final results are by no means based completely on theoretically rigorous procedures, they do represent detailed consideration of all important effects and contributions utilizing theoretically justifiable concepts.

Calculations are carried out for four Mach numbers: $\sqrt{2}$, 2, 2.5, and 3. It may be noted at this point that the range of Mach numbers considered includes the cases where the wing and tail surfaces have subsonic leading edges, supersonic leading edges, and combinations of the two.

Results for the stability derivatives are presented relative to a body system of axes maintaining, however, the usual stability convention for denoting positive forces and moments. (See fig. 2.) Radian measure is used throughout for the derivatives.

STABILITY DERIVATIVES DUE TO ANGLE OF ATTACK

General Considerations

The body, wing, and horizontal tail are all assumed to be at a small angle of attack. The lift on the isolated body is concentrated mainly over the forward portion; the exposed panels of both the wing and horizontal tail in addition to carrying their own lift are affected by the presence of the body and in turn induce some lift on the body. There is also, of course, the downwash effect from the wing which decreases the lift effectiveness of the horizontal tail. Fortunately, for the angle-of-attack case there is, relatively speaking, considerable published information to be drawn upon for purposes of estimating the various contributions. The isolated wing and tail surfaces, both of which are modified delta plan forms, are treated in references 1, 2, and 3; wing-body and body-wing interference effects may be estimated most conveniently and apparently quite satisfactorily for circular bodies of revolution by use of references 4, 5, and 6. The effect of the isolated body is difficult to determine accurately because of the cross-sectional deviations of the airplane fuselage from the theoretically treated bodies of revolution. However, slender-body theory for bodies of revolution in conjunction with some results obtained in references 7 and 8 for other types of bodies enable a qualitative evaluation of the effects of the isolated body and its influence on the mutual interference effects between body and wing or tail surfaces. The induced flow from the wing has been treated in some detail by various investigators (see, for example, refs. 9 to 12) and hence the net contribution of the horizontal tail may be readily calculated. It appears, therefore, that by judicious use of the available information theoretically justifiable and reliable estimates of the derivatives $C_{L\alpha}$ and $C_{m\alpha}$ may be anticipated.

Detailed Considerations and Results

The lift-curve slope $C_{L\alpha}$ and the pitching moment due to angle of attack (i.e., stability derivative $C_{m\alpha}$) for the isolated wing and isolated horizontal tail are directly obtainable from reference 1 for the subsonic leading-edge cases and from references 2 and 3 for the supersonic leading-edge cases. Although a number of methods were investigated in order to estimate the interference effects between wing and fuselage (and between horizontal tail and fuselage), the results obtained agreed in general with those predicted by use of references 4 to 6, hence the details of the calculations will not be presented. The lift on the isolated fuselage was calculated to be slightly greater than that predicted by slender-body theory. Inasmuch as slender-body theory fails to predict any lift on the cylindrical portion of a cone-cylinder fuselage combination, it

is felt that an estimate based in part on the results given in reference 7 is more realistic. The downwash in the vicinity of the horizontal tail was calculated using the procedures indicated in references 9 and 10. The assumption (which for this particular configuration is quite reasonable) is made that the vortex sheet remains flat in the vicinity of the tail. Values of the downwash were obtained at several stations behind the apex of the horizontal tail and then averaged over the horizontal tail surface to form an "effective" downwash velocity. Figure 3 presents the variation of the downwash factor $w/\alpha V$ with Mach number. The corresponding induced angle of attack at the tail was then added to the geometric angle of attack of the tail and the resulting lift (neglecting the presence of the body) was calculated using references 1 and 2. Interference effects between horizontal tail and fuselage were calculated in a manner similar to that used for the wing-fuselage interference effects. The net result of adding the lift contributions of all components taking into account the calculated interference and induced flow effects, that is, the estimated lift-curve slope of the complete airplane configuration, is presented in figure 4 together with some breakdown results. The ordinate is the lift-curve slope $C_{L\alpha}$ based on a reference area S that includes both the area of the exposed wing panels and the masked (by the fuselage) portion of the wing extended to the fuselage center line. As mentioned previously (see section entitled "SCOPE"), actual calculations were carried out for four values of the abscissa Mach number ($\sqrt{2}$, 2, 2.5, and 3) and the final curve faired accordingly.

Calculation of the pitching moment due to angle of attack is a bit more difficult inasmuch as detailed information for the incremental center-of-pressure shifts or incremental pitching moments due to the various component effects discussed previously (for $C_{L\alpha}$) is lacking. Reference 5 considers the interference effects between wing and fuselage (and between horizontal tail and fuselage). Calculations of the other effects were made by first assuming center-of-pressure locations (based on approximate lift distributions due to each effect or component) and then evaluating the significance of varying the assumed center-of-pressure locations through a reasonable range. Inasmuch as the pitching moment is significantly different from zero, this method of "averaging" the results should yield satisfactory estimates. The resulting pitching-moment derivative for the complete configuration expressed in derivative form is presented in figure 5; some breakdown results are also shown. The stability derivative $C_{m\alpha}$ is based on the reference area S and the mean aerodynamic chord \bar{c} . Moments are taken about a center-of-gravity location assumed to be at 32 percent of the mean aerodynamic chord.

STABILITY DERIVATIVES DUE TO PITCHING

General Considerations

Aside from calculations for isolated wings (e.g., refs. 1, 3, 13, and 14) there is relatively little theoretical information available concerning the pitching-moment derivatives C_{m_q} and $C_{m_{\dot{\alpha}}}$. Some results for various types of isolated bodies of revolution are given in references 15 and 16. Reference 17 considers time-dependent downwash at the tail, which requires knowledge of the downwash due to steady pitching as well as that due to constant angle of attack. Calculations for angle-of-attack downwash are available from a number of sources (see section regarding angle of attack); data on steady-pitching downwash are lacking although rather simplified approximations have been used to advantage in the past. More detailed calculations of the downwash due to steady pitching and the downwash due to linear angle-of-attack variation with time (i.e., constant $\dot{\alpha}$) are in progress. Although subject to restrictions on the permissible configurations, reference 18 is quite useful in determining wing-body effects. Thus, the estimation of the derivatives C_{m_q} and $C_{m_{\dot{\alpha}}}$ for an arbitrary complete configuration is dependent on essentially the material and references given above. Although the present wealth of published or near-published theoretical studies for pitching motion is in no way comparable to that for angle of attack, it has been shown in an unpublished analysis to be adequate for the prediction of the level or magnitude of $C_{m_q} + C_{m_{\dot{\alpha}}}$ for a number of missile configurations. In view of this evidence there is reason to believe that the theoretical estimates of the pitching derivatives for the present configuration are fairly realistic in spite of the fact that its geometric variations from theoretically treated cases are significant in some respects.

Detailed Considerations and Results

The derivatives C_{m_q} and $C_{m_{\dot{\alpha}}}$ for the isolated wing and horizontal tail are directly obtainable from reference 1 for the subsonic-leading-edge cases. For the case of a supersonic leading edge C_{m_q} is given in reference 3 and $C_{m_{\dot{\alpha}}}$ in an unpublished analysis. (Actually the wing and horizontal tail are so near to being delta plan forms that the formula given in reference 14 for $C_{m_{\dot{\alpha}}}$ may be used without significant error.)

In calculating the wing-body effects by use of reference 18, the wing trailing edge was modified slightly to form a delta wing with the same area as the actual wing. The tail contributions to the derivatives C_{m_q}

and $C_{m\dot{\alpha}}$ were calculated from simplified approximations based in part on reference 17. The tail contribution to $C_{m\dot{q}}$ was obtained by adding to the isolated-tail value a correction for the wing downwash based on equation (21) of reference 17. Inasmuch as the horizontal tail of the airplane configuration is only a short distance behind the wing, the degree of accuracy of this approximation required consideration. For a subsonic-edge delta wing at Mach number $\sqrt{2}$, values of w_q based on more exact procedures were compared with those used herein. The resulting correction to $C_{m\dot{q}}$ based on the more exact approach did not result in a significant change. The tail contribution to $C_{m\dot{\alpha}}$ was calculated from an unpublished analysis which was based on a simplified approximation to the method presented in reference 17. The downwash due to $\dot{\alpha}$ also checked fairly well at $M = \sqrt{2}$ with more exact calculations. Summation of the results obtained for the various isolated components, components in combination, and induced-flow effects yielded the curve shown in figure 6 for the damping in pitch $C_{m\dot{q}} + C_{m\dot{\alpha}}$ of the complete configuration. A partial breakdown of the results is also indicated. It is of interest to point out that the contribution from the $\dot{\alpha}$ term alone is unstable for this particular configuration but fortunately is small in comparison with the damping effect due to the steady pitching component.

STABILITY DERIVATIVES DUE TO STEADY ROLLING

General Considerations

In order to estimate with a reasonable degree of accuracy the stability derivatives associated with steady rolling motion (C_{l_p} , C_{Y_p} , and C_{n_p}) for a complete configuration, a prime requirement is to have reliable knowledge of induced-flow effects. Unfortunately, there is a lack of information with regard to this aspect. Results for isolated wings (and horizontal tails) of various plan forms are available in a number of papers (e.g., refs. 19 to 23); wing-body and tail-body interference effects for restricted types of configurations are treated in references 24 to 26. Various types of tail configurations are considered in references 27 to 29. An attempt to take induced-flow phenomena into account in estimating the derivative C_{l_p} for a missile configuration was made in reference 30, but the results were not too general in nature nor was the accuracy of the procedure involved satisfactory. Thus, although for the previous motions treated (angle of attack and pitching) experience had shown the methods employed therein in estimating the

derivatives to be reliable, such is not the situation for the case of rolling. Consequently, detailed attention will be given to the derivation of expressions relating to induced-flow calculations as well as to the estimation of the contributions due to the pertinent airplane components and components in combination.

Detailed Considerations and Results

Wing loading.- In order to obtain reliable force and moment derivatives for a wing-body-tail configuration in roll, the effect of the flow field on the tail must be considered. Since the flow field is determined by the span loading, it is desirable that it (the span loading) be calculated as accurately as possible. Large changes in the spanwise loading near the root of a wing which might be occasioned by the presence of a body or end plate may cause a noticeable difference in the flow field, yet affect the damping of the wing itself only slightly. For this reason it was considered necessary to modify the isolated-wing loading to take into account the presence of the body.

In addition to this "end-plate" effect, the presence of the body causes a change in the position of the leading Mach lines on the wing (as compared to the isolated-wing case). Whereas for the isolated-wing situation the leading Mach lines emanate from the wing apex, the leading Mach lines for the wing-body combination originate at the intersections of the wing leading edge with the body.

In order to approximate the effect on the wing loading of superposing a body (and the corresponding change in Mach line position), a rather straight-forward procedure has been followed. First, the span loading in roll over a wing composed of the two wing panels exterior to the body and joined together at their roots was determined by use of references 31 and 32. Then the two panels were separated and placed on the body. Since the previously determined span loading for the rolling wing was predicated on the wing rolling about its axis of symmetry, that is, the half-wings rolling about their root chords, an additional loading was added to compensate for the greater distance of each point on the wing from the roll axis. (The angle-of-attack distribution which gives rise to this additional loading is constant and equal to the quantity $\rho a/V$.) This procedure did not predict the loading on the body. In order to complete this portion of the loading curve, a straight line was drawn between the finite values at the wing-body juncture and zero at the roll axis. The resultant span loadings for the wing-body configuration at Mach numbers of $\sqrt{2}$, 2, 2.5, and 3 are shown in figure 7. For purposes of comparison, figure 8 presents the loading at Mach number $\sqrt{2}$ obtained by the present method and the corresponding loading for a fictitious isolated wing formed by extending the leading and trailing edges of the exposed wing panels to the center line. It will be noted that the loading at the

root of the wing predicted by the present method is slightly higher than that obtained for the isolated wing. As the distance from the root along the span increases, the difference between these two loadings decreases. Further calculations and comparisons at the higher Mach numbers indicated insignificant differences between the modified loading (present method) and isolated wing loading at all spanwise stations.

As expected, it was found that the improved or modified loadings yielded wing-body force and moment derivatives that differed only slightly from those obtained by use of isolated-wing loadings. However, it appeared that the modified loading curves would produce a noticeable change in the flow-field calculations, especially at the lower Mach numbers, and hence they have been utilized in all such calculations.

Flow-field theory.- There are many papers which present general formulas for the potential in space due to a thin lifting surface. In most cases these formulas are extremely difficult to evaluate. It becomes necessary, therefore, to utilize some approximation which may be more easily evaluated and which lends itself to numerical calculations. Reference 9 indicates that a lifting line can be used as a very good approximation for most downwash problems. A similar statement regarding sidewash problems may not be made since there are no exact expressions available for the sidewash behind rolling wings. It might be noted, however, that an approach somewhat like the above was used in reference 33 for calculating sidewash behind rolling wings traveling at subsonic speeds and very good agreement with experimental results was realized.

Taken together, references 34, 9, and 12 represent a fairly thorough study of the lifting-line approximation, especially with regard to downwash problems, and show that bent lifting lines will probably give the best results for swept and triangular wings. The shape of the bent lifting line most often used in these papers and also used herein consists of a pair of straight lines connecting the midpoints of the root and tip chords of the wing. The potential due to a slanted lifting line of this type may be obtained from reference 34 (certain errors present therein having been corrected in the following equation):

$$\phi = \frac{\Gamma(y_1)}{2\pi} \tan^{-1} \frac{z\sqrt{X^2 - B^2(y^2 + z^2)}}{YX - \frac{z^2}{m} - \frac{y^2}{m}} \Big|_{h_1}^{h_2}$$

$$\frac{1}{2\pi} \int_{h_1}^{h_2} \frac{d\Gamma(y_1)}{dy_1} \tan^{-1} \frac{z\sqrt{X^2 - B^2(y^2 + z^2)}}{YX - \frac{z^2}{m} - \frac{y^2}{m}} dy_1 \quad (1)$$

where the equation of the lifting line is

$$x_1 = \frac{y_1 + k}{m}$$

(See fig. 9 for pertinent symbols, etc.) When $\frac{d\Gamma(y_1)}{dy_1}$ is zero, equation (1) becomes

$$\phi = \frac{\Gamma}{2\pi} \tan^{-1} \frac{z\sqrt{X^2 - B^2(Y^2 + z^2)}}{YX - \frac{z^2}{m} - \frac{Y^2}{m}} \Bigg|_{h_1}^{h_2} \quad (2)$$

which might be considered as the potential in space (at a point (x,y,z)) of a finite bent vortex of constant strength. A number of these superposed on one another can be used to approximate the potential in space of a lifting line with any prescribed lift distribution, for example, such as those previously calculated (fig. 7) for the rolling wing-body of the configuration (see ref. 34).

From equation (2) the sidewash and downwash due to a bent vortex are readily obtained by taking the derivative with respect to y and z . The following results are obtained:

$$v = \phi_y = \frac{\Gamma}{2\pi} \left\{ \frac{\frac{zY}{m}(2X^2 - B^2Y^2 - B^2z^2) - zX(X^2 - B^2z^2)}{\sqrt{X^2 - B^2(Y^2 + z^2)} \left[\left(YX - \frac{z^2}{m} - \frac{Y^2}{m} \right)^2 + z^2(X^2 - B^2Y^2 - B^2z^2) \right]} \right\} \Bigg|_{h_1}^{h_2} \quad (3)$$

and

$$-w = -\phi_z = -\frac{\Gamma}{2\pi} \left\{ \frac{YX^3 + \frac{X^2}{m}(z^2 - Y^2) - B^2YX(Y^2 + 2z^2) + \frac{B^2Y^2}{m}(z^2 + Y^2)}{\sqrt{X^2 - B^2(Y^2 + z^2)} \left[\left(YX - \frac{z^2}{m} - \frac{Y^2}{m} \right)^2 + z^2(X^2 - B^2Y^2 - B^2z^2) \right]} \right\} \Bigg|_{h_1}^{h_2} \quad (4)$$

Since the loading on a rolling wing is antisymmetrical, the induced sidewash velocity from each panel is in the same direction and equal in the $y = 0$ plane (the plane of the vertical tail). For this reason, it is necessary to calculate only the sidewash from one panel (using eq. (3)) and double it. To calculate the total downwash at any arbitrary point on the horizontal tail requires that the contribution from both panels be determined. Hence it is necessary to obtain an expression for ϕ_z when bent lines have negative slopes. Inasmuch as m and k are defined as absolute values, this condition is represented by the following equation for the lifting line:

$$x_1 = \frac{-y_1 + k}{m}$$

Appropriate modification of the potential (eq. (2)) and differentiation with respect to z yields

$$-w = -\phi_z = -\frac{\Gamma}{2\pi} \left[\frac{YX^3 - \frac{X^2}{m}(z^2 - Y^2) - B^2YX(Y^2 + 2z^2) - \frac{B^2Y^2}{m}(z^2 + Y^2)}{\sqrt{X^2 - B^2(Y^2 + z^2)} \left[\left(YX + \frac{z^2}{m} + \frac{Y^2}{m} \right)^2 + z^2(X^2 - B^2Y^2 - B^2z^2) \right]} \right] \Bigg|_{h_1}^{h_2} \quad (5)$$

Flow-field calculations.- Equation (3) can be utilized to formulate an approximate expression for the sidewash due to a series of constant-strength, horseshoe vortices spaced along a line so as to represent as closely as possible some prescribed span loading. This expression is

$$v = -\sum_{i=0}^n \frac{\Gamma(y_{i+1}) - \Gamma(y_{i-1})}{4\pi} \frac{\frac{zy_i}{m}(2X_1^2 - B^2Y_1^2 - B^2z^2) - zX_1(X_1^2 - B^2z^2)}{\sqrt{X_1^2 - B^2(Y_1^2 + z^2)} \left[\left(Y_1X_1 - \frac{z^2}{m} - \frac{Y_1^2}{m} \right)^2 + z^2(X_1^2 - B^2Y_1^2 - B^2z^2) \right]} \quad (6)$$

where $Y_1 = y - y_1$ and $X_1 = x - x_1$. The subscript i takes on all integral values from 0 to n . Since span load distributions are usually determined from prescribed angle-of-attack distributions and since the

primary purpose of calculating the flow field behind the wing is to determine the induced loads on the tail, it is advantageous to write equation (6) in the following form:

$$\frac{v/V}{\frac{pb}{2V}} = - \sum_{i=0}^n \frac{\left[\frac{\Gamma(y_{i+1})}{p(b/2)^2} - \frac{\Gamma(y_{i-1})}{p(b/2)^2} \right] \left[\frac{\bar{z}\bar{y}_i}{m} (2\bar{x}_i^2 - B^2\bar{y}_i^2 - B^2\bar{z}^2) - \bar{z}\bar{x}_i (\bar{x}_i^2 - B^2\bar{z}^2) \right]}{4\pi \sqrt{\bar{x}_i^2 - B^2(\bar{y}_i^2 + \bar{z}^2)} \left[\left(\bar{y}_i\bar{x}_i - \frac{\bar{z}^2}{m} - \frac{\bar{y}_i^2}{m} \right)^2 + \bar{z}^2 (\bar{x}_i^2 - B^2\bar{y}_i^2 - B^2\bar{z}^2) \right]} \quad (7)$$

From this equation the induced angle of sidewash v/V per unit $pb/2V$ is arrived at directly. The bar simply denotes that the quantity is non-dimensional with respect to the wing semispan. Following this same procedure, the induced angle of downwash per unit $pb/2V$ at any point in space behind a rolling wing may be obtained from equations (4) and (5) as

$$\begin{aligned} - \frac{w/V}{\frac{pb}{2V}} = & - \sum_{i=n_1}^0 \frac{\left[\frac{\Gamma(y_{i+1})}{p(b/2)^2} - \frac{\Gamma(y_{i-1})}{p(b/2)^2} \right] \left[\bar{y}_i\bar{x}_i^3 - \frac{\bar{x}_i^2}{m} (\bar{z}^2 - \bar{y}_i^2) - B^2\bar{y}_i\bar{x}_i (\bar{y}_i^2 + 2\bar{z}^2) - \frac{B^2\bar{y}_i^2}{m} (\bar{z}^2 + \bar{y}_i^2) \right]}{4\pi \sqrt{\bar{x}_i^2 - B^2(\bar{y}_i^2 + \bar{z}^2)} \left[\left(\bar{y}_i\bar{x}_i + \frac{\bar{z}^2}{m} + \frac{\bar{y}_i^2}{m} \right)^2 + \bar{z}^2 (\bar{x}_i^2 - B^2\bar{y}_i^2 - B^2\bar{z}^2) \right]} + \\ & \sum_{i=0}^{i=n_2} \frac{\left[\frac{\Gamma(y_{i+1})}{p(b/2)^2} - \frac{\Gamma(y_{i-1})}{p(b/2)^2} \right] \left[\bar{y}_i\bar{x}_i^3 + \frac{\bar{x}_i^2}{m} (\bar{z}^2 - \bar{y}_i^2) - B^2\bar{y}_i\bar{x}_i (\bar{y}_i^2 + 2\bar{z}^2) + \frac{B^2\bar{y}_i^2}{m} (\bar{z}^2 + \bar{y}_i^2) \right]}{4\pi \sqrt{\bar{x}_i^2 - B^2(\bar{y}_i^2 + \bar{z}^2)} \left[\left(\bar{y}_i\bar{x}_i - \frac{\bar{z}^2}{m} - \frac{\bar{y}_i^2}{m} \right)^2 + \bar{z}^2 (\bar{x}_i^2 - B^2\bar{y}_i^2 - B^2\bar{z}^2) \right]} \quad (8) \end{aligned}$$

where n_1 is associated with negative values of y_i and n_2 is associated with positive values of y_i . It should be noted that in equation (8) the parameters i , n_1 , and n_2 are always positive. The expression for x_i corresponding to positive values of y_i is

$$x_i = \frac{y_i + k}{m}$$

and that corresponding to negative values of y_1 is

$$x_1 = \frac{-y_1 + k}{m}$$

Seventeen horseshoe vortices on each half-wing were used to approximate the span load distribution (expressed in terms of Γ in the equations). (See fig. 10.) Calculations of the induced angles of sidewash and downwash (eqs. (7) and (8), respectively) were carried out for a number of longitudinal locations along the tail surfaces. For each longitudinal location considered, the induced angles of sidewash and downwash were obtained at the root, tip, and intermediate spanwise positions of the appropriate tail surfaces. By means of an averaging process, resultant curves for the spanwise variation of the "effective" induced angles were obtained. The results at various Mach numbers for the spanwise variation in downwash angle for the horizontal tail are presented in figure 11; corresponding results for the sidewash angle for the vertical tail are presented in figure 12. It should be noted that the chordwise variations of the induced angles on the tails were small and hence the curves obtained by the averaging process represent fairly accurately the spanwise variation at any longitudinal station. It should also be noted that the effect of the body on the flow field behind the wing has been assumed to be small and therefore neglected.

Tail loads, forces, and moments.- To determine the induced pressures and the corresponding induced loadings on the tail surfaces by the exact methods requires detailed knowledge of the induced angles of sidewash and downwash at each point of the pertinent tail surface. Furthermore, derivation of the induced pressures from the induced-angle distributions entails considerable difficulties except for the most simple cases. To utilize a theoretically rigorous approach in the present investigation would obviously necessitate an almost prohibitive amount of work. An alternate method of attack on the problem is to determine the desired induced loadings on the tail surfaces by utilizing loadings that have been previously obtained in references 31 and 32 for isolated wings undergoing various motions. In order to do this, however, it is necessary that the induced-angle distributions for the tail be defined by constant or linear (zero value at origin) expressions as is the case, for example, of an isolated wing at a constant angle of attack, in steady rolling, or in steady pitching. Inasmuch as superposition of these solutions is permissible, the criterion for enabling the utilization and application of isolated-wing loadings to the calculation of induced tail loadings is that the induced angles of sidewash and downwash on the tail surfaces be approximated by arbitrary straight lines. While it may not be possible to represent accurately with straight lines the induced angles of sidewash and downwash for all configurations, it does seem that for the majority of cases this may be done without incurring a large percentage error in

the induced loading. When there is little or no longitudinal variation in the induced angles of downwash and sidewash (as has been stated in the previous section to be the situation for the configuration under study) the induced loading may be built up solely of two load distributions, one corresponding to that obtained for a wing at a constant angle of attack and the other corresponding to that obtained for a wing in steady rolling. This point will be more fully explained in the discussion which follows.

The straight-line approximation of the average induced-downwash and induced-sidewash curves for the tail surfaces of the configuration is indicated in figures 11 and 12. For convenience, a typical curve has been selected (see fig. 13) to indicate how the induced-angle distribution may be broken up into two components, one component being a horizontal line defined by

$$\left(\frac{v/V}{\frac{pb}{2V}}\right)_1 = k_1 \quad (9)$$

and the other component being a line of nonzero slope passing through the origin:

$$\left(\frac{v/V}{\frac{pb}{2V}}\right)_2 = k_2 \frac{z}{b/2} \quad (10)$$

The difference $k_1 - k_2 \frac{z}{b/2}$ is the actual induced-angle distribution (as approximated by a straight line). It is readily seen that the component angle distributions defined by equations (9) and (10) are similar to the distributions obtained for isolated wings at a constant angle of attack and in steady rolling, respectively. Taking into account the constants used to nondimensionalize the quantities given by equations (9) and (10), the induced load distribution for each component may easily be obtained from charts presented in references 31 and 32.

The induced load distributions thus far obtained have utilized wing loadings that are applicable to one panel of a symmetrical wing. It is of course necessary to modify these results so as to account for the mutual interference effects between the horizontal and vertical tail surfaces as well as to simulate in some manner the proper end-plate effects caused by the presence of the body. Inasmuch as the isolated tail surfaces performing a steady roll have load distributions which must also be modified to take into account interference phenomena, it is more

convenient to add together the uncorrected induced load distributions to the isolated tail load distributions and then correct all load distributions simultaneously. The load distribution due to the isolated tail surfaces in roll has been obtained directly from references 31 and 32, once again considering each tail panel as one-half of a symmetrical wing.

Inasmuch as there is little information at supersonic speeds concerning horizontal-vertical tail combinations in roll with the exception of "slender" arrangements (ref. 28), the interference effects must be evaluated in an approximate manner. Since the tail surfaces of the present configuration are highly swept and of moderate aspect ratio, it has been found advantageous to modify the previously obtained load distributions by interference correction factors based on results obtained for slender tail arrangements in steady roll (ref. 28) and slender tail arrangements at constant sideslip (ref. 35).

Before discussing the interference correction factors in detail it should be remembered that each induced load distribution was subdivided into two component load distributions, that is, an angle-of-attack distribution (which is directly comparable to a load distribution due to constant sideslip for a vertical tail) and a steady-roll distribution. Inasmuch as the mutual interference effects are different for the rolling and angle-of-attack (or sideslip) cases, each of these load distributions must be modified in a different manner. The rolling component of the induced load distributions may of course be combined with the isolated-rolling-tail load distributions for purposes of applying the interference correction factor.

For the rolling load distributions, interference correction factors based on slender-body theory have been used. To obtain these slender-body correction factors, the tail system of the configuration under study has been approximated by an equivalent tail system composed of half-delta panels intersecting in a common chord at the roll axis. The areas of both the horizontal and vertical tails in the equivalent system were essentially unchanged from those in the original configuration. Actually the vertical tail which is by far the more important contributor to the rolling moment and the sole contributor to the yawing moment was changed only slightly from its original shape. With the ratio of the vertical-tail span to the horizontal-tail span known for this equivalent tail system, correction factors have been obtained from references 28 and 35 and applied to the uncorrected load distributions in the following manner: Let L_0' be the uncorrected rolling load component and L_1' be the uncorrected angle-of-attack (i.e., sideslip) load component;

For the vertical tail,

$$\left(\int \begin{Bmatrix} L_0' \\ L_0'z \\ L_0'x \end{Bmatrix} dz \right) \left(\frac{\begin{Bmatrix} Y \\ L' \\ N \end{Bmatrix} \text{ of vertical panel of slender inverted T-tail in roll}}{\begin{Bmatrix} Y \\ L' \\ M \end{Bmatrix} \text{ of one panel of a slender triangular wing in roll}} \right) \quad (11)$$

and

$$\left(\int \begin{Bmatrix} L_1' \\ L_1'z \\ L_1'x \end{Bmatrix} dz \right) \left(\frac{\begin{Bmatrix} Y \\ L' \\ N \end{Bmatrix} \text{ of vertical panel of slender inverted T-tail in sideslip}}{\begin{Bmatrix} Y \\ L' \\ M \end{Bmatrix} \text{ of one panel of a slender triangular wing at an angle of attack}} \right) \quad (12)$$

For the horizontal tail,

$$\left(\int L_0'y dy \right) \left(\frac{L' \text{ of horizontal panel of slender inverted T-tail in roll}}{L' \text{ of one panel of a slender triangular wing in roll}} \right) \quad (13)$$

The rolling moment contributed by the angle-of-attack component of the load distribution on the horizontal tail is proportional to

$$\int L_1'y dy \quad (14)$$

There is also an induced loading on the horizontal tail due to the induced angle-of-attack component of the load acting on the vertical tail. This effect would be in addition to the result given by expression (14) and has been calculated by use of reference 35.

The expressions (11) to (14) must of course be nondimensionalized and combined properly to yield tail forces and moments. The tail contributions to the stability derivatives C_{l_p} , C_{Y_p} , and C_{n_p} may then readily be obtained by use of the conventional definitions.

In determining the total forces and moments contributed by the tail surfaces, however, only those portions of the loads exterior to the body (body boundary defined by $\frac{z}{b/2} = 0.106$ for the case of the vertical tail) were integrated (see expressions (11) to (14)). It was assumed that the resultant of the forces and moments acting on the body, that is, those due to the isolated body in roll, the induced effects, and so forth, was very small and hence neglected.

It is possible to compare the accuracy of some of the approximations used with calculations based on rigorous applications of linearized theory. Inasmuch as these checks deal with the angle-of-attack component of the induced load on the vertical tail (i.e., sideslip effect), the comparisons will be made in a subsequent section of the report dealing with the sideslipping motion.

Specific derivatives.- The value of C_{l_p} due to the wing-body combination is readily obtained from the loadings which were discussed in a previous section and presented in figure 7. The addition of the wing-body contribution to the total tail contribution yields the damping-in-roll derivative C_{l_p} for the complete configuration (fig. 14). It is interesting to note that the net tail contribution to the derivative C_{l_p} was found to be insignificant through the Mach number range considered. For this particular configuration, the flow field and other interference effects almost entirely nullified the damping of the isolated tail unit. Thus the curve shown for the complete configuration is very close to the result obtained for the wing-body contribution.

Inasmuch as the configuration was assumed to be at zero geometric angle of attack, there were no suction forces on the wing leading edge at Mach numbers for which the edge was subsonic. (At Mach numbers for which the wing leading edge is supersonic, there would be no suction forces present at any angle of attack.) Thus the derivatives C_{Y_p} and C_{n_p} are composed solely of the tail contributions. The variation of the stability derivative C_{Y_p} with Mach number for the complete configuration is shown in figure 15; some pertinent breakdown results are also included.

In order to obtain the stability derivative C_{n_p} , each of the previously discussed load components acting on the vertical tail was isolated

and the center-of-pressure location for each component was determined at the four Mach numbers considered. (It is interesting to note that the center-of-pressure locations for all components and at all Mach numbers did not vary too greatly from the $3/4$ -root-chord position.) Each load component was then multiplied by the appropriate arm length (measured from the center of gravity to the calculated center-of-pressure location) and the results added to obtain the total yawing moment. The variation of the corresponding derivative C_{n_p} with Mach number is presented in figure 16. The sidewash effect on the derivative C_{n_p} (and C_{Y_p}) is quite marked; note the reversal in sign near Mach number 1.6.

STABILITY DERIVATIVES DUE TO CONSTANT SIDESLIP

General Considerations

The information available pertinent to the theoretical calculation at supersonic speeds of sideslip effects for complete configurations is of relatively scant nature. Results for isolated wings without geometric dihedral are available for combined sideslip and angle-of-attack motion (refs. 36, 37, and 38). Wings with geometric dihedral are considered in references 39 and 40. For bodies of revolution, results available for angle of attack (e.g., refs. 7 and 41) may of course be applied to the sideslip motion. For fuselage shapes with noncircular cross sections and abrupt contour changes there is very little information. Some results of investigations for various tail configurations in sideslip are given in references 35, 41, and 42; other information is as yet unpublished. Flow-field and component interference effects have not received any significant attention to date in the literature. It is seen, therefore, that considerable additional research is required before accurate estimation of the stability derivatives due to sideslip for arbitrary complete configurations can be obtained. In analyzing the present configuration the most important effects have been accounted for by utilizing the available theory in conjunction with several semiempirical approximations. The reasonableness of the approximations is demonstrated wherever possible.

Detailed Considerations and Results

The forces and moments produced by the vertical tail at an angle of sideslip may be obtained by a procedure analogous to that used in treating the angle-of-attack component of the induced load on the vertical tail due to steady rolling. (See section for rolling motion entitled "Tail Loads, Forces, and Moments.") From this angle-of-attack component, forces and moments on the sideslipping tail may be obtained in a fairly simple manner.

While before the angle of attack was given in terms of $pb/2V$ (see eq. (9)) and only a fractional part of the loading due to a fictitious angle β was used, now the actual angle of sideslip is β and the entire loading must of course be considered. It should be noted that end-plate effects on the load distribution due to sideslip have also been taken into account in treating the angle-of-attack component of the induced load due to rolling motion and hence no further consideration of them is necessary.

From the loadings just discussed, contributions of the tail unit to the stability derivatives $C_{Y\beta}$, $C_{n\beta}$, and $C_{l\beta}$ may be readily obtained. The accuracy of the end-plate corrections made in obtaining the vertical-tail contributions to the sideslip derivatives may be examined in the light of some rigorous results available for isolated vertical tails with zero and complete end plates. Values for the tail contributions obtained herein using wing loadings corrected for end-plate effects should, of course, fall between these two limiting cases.

For isolated vertical tails with supersonic leading edges, both the zero- and complete-end-plate solutions for $(C_{Y\beta})_t$, $(C_{n\beta})_t$, and $(C_{l\beta})_t$ are presented in reference 42. For the subsonic-leading-edge condition, complete- and zero-end-plate boundaries for $(C_{Y\beta})_t$ and $(C_{n\beta})_t$ may be obtained by use of the $C_{L\alpha}$ and $C_{m\alpha}$ expressions for isolated wings presented in reference 1. (The angle-of-attack solution for a wing is comparable to the complete-end-plate case for a vertical tail in sideslip.) The complete-end-plate solution for $(C_{l\beta})_t$ has been derived in an unpublished analysis. The zero-end-plate boundaries for the derivatives $(C_{Y\beta})_t$, $(C_{n\beta})_t$, and $(C_{l\beta})_t$ that are valid at Mach numbers for which the tail leading edge is subsonic may be obtained from expressions presented in reference 43.

The calculated tail contribution (which includes a finite end-plate effect) to the stability derivative $C_{Y\beta}$ is compared with the zero- and complete-end-plate boundaries in figure 17; the reasonableness of the approximations used in the calculation is readily apparent. Similar comparisons for the tail contributions to the stability derivatives $C_{n\beta}$ and $C_{l\beta}$ yielded equally satisfactory results. (It should be mentioned that the zero-end-plate boundary for Mach numbers corresponding to subsonic leading edges was calculated from ref. 43, with the vertical tail being slightly modified to form a half-delta of equivalent area.)

In calculating the isolated-body effects, it was realized that the airplane fuselage would probably have a relatively large side force associated with the sideslip motion. (As can be seen from fig. 1, the cross sections of the rearward part of the body are almost rectangular in shape.) Unfortunately most of the existing information concerning bodies is restricted to slender bodies of revolution. No formulas are available at present which will predict the forces and moments on yawed bodies with noncircular cross sections and abrupt contour changes similar to the body considered herein. It becomes necessary therefore to approximate the body by an equivalent body of revolution. Obviously there are any number of circular body shapes which could conceivably represent an "equivalent" body. Thus any theoretical approximation based on conventional bodies of revolution would be subject to considerable uncertainties. In order to minimize the error involved, two estimates of the body contribution were calculated; one that was felt to be an underestimate and one an overestimate, both being calculated from slender-body theory (for example, see ref. 41). The resulting two values for $C_{Y\beta}$ were averaged and this average value was used for the body effect. A similar sort of averaging process was used in estimating the longitudinal center-of-pressure location in order to obtain the body contribution to $C_{n\beta}$. The body contribution to $C_{l\beta}$ is very small and hence can be neglected. In connection with these isolated-body effects, it should be borne in mind that any inaccuracies present in the body estimates would of course affect the total $C_{Y\beta}$ estimate more than the total $C_{n\beta}$ or total $C_{l\beta}$ estimates because of the relatively short moment arm involved for the body as compared to that of the vertical tail. Variations of the derivatives $C_{Y\beta}$, $C_{n\beta}$, and $C_{l\beta}$ with Mach number for the complete configuration are shown in figures 18, 19, and 20, respectively; some breakdown results are also included.

STABILITY DERIVATIVES DUE TO STEADY YAWING

General Considerations

With regard to steady yawing motion, there is an almost complete lack of the information required for estimating stability derivatives for complete configurations. In fact, this statement is almost equally applicable to isolated components. Isolated wings have been treated in references 1, 44, 45, and 46 but some of the results obtained therein are based on fairly crude approximations and must be considered of only qualitative value. For isolated bodies of revolution the relatively few calculations available for steady pitching motion (e.g., refs. 15 and 16) may of course be applied to the case of steady yawing. For fuselage shapes

other than bodies of revolution there is essentially no information. Wing-body interference effects and flow-field calculations have not been considered to date. In analyzing the present configuration, a number of semiempirical approximations have been employed in estimating the more important effects. Calculations for various tail configurations are now in progress and these have been utilized to some extent in checking the reasonableness of the approximations for the tail-body contribution.

Detailed Considerations and Results

In the absence of information concerning the end-plate effects of bodies and horizontal tails on yawing vertical tails, two methods were used to evaluate the vertical-tail contribution to the stability derivatives C_{Y_r} , C_{N_r} , and C_{L_r} . The first method was an approximation based on the results obtained for the sideslipping motion and utilized the following relationships

$$(C_{Y_r})_t = - \frac{\partial(C_{Y_t})}{\partial\beta} \frac{\partial\beta}{\partial \frac{rb}{2V}} = -(C_{Y\beta})_t \frac{\partial\beta}{\partial \frac{rb}{2V}} \quad (15)$$

where the minus sign is introduced to maintain the conventional system of positive forces and moments and

$$\beta = \frac{rl}{V} = \frac{rb}{2V} \frac{l}{b/2}$$

It is clear then that

$$\frac{\partial\beta}{\partial \frac{rb}{2V}} = \frac{l}{b/2}$$

and hence

$$(C_{Y_r})_t = -(C_{Y\beta})_t \frac{l}{b/2} \quad (16)$$

Analogous procedures yield

$$(C_{nr})_t = -(C_{n\beta})_t \frac{l}{b/2} \quad (17)$$

and

$$(C_{lr})_t = -(C_{l\beta})_t \frac{l}{b/2} \quad (18)$$

In the preceding equations l is the distance between the center of gravity of the airplane and the center of pressure of the vertical tail (in the presence of the body) for the sideslip motion.

A second method of estimating the tail contribution to the yawing derivatives is to calculate the two limiting cases (similar to what was done for sideslip) corresponding to zero- and complete-end-plate situations and then obtain an average value. In order to obtain the complete end-plate solutions for C_{Y_r} and C_{N_r} , the results for C_{L_q} and C_{m_q} available for wings may be utilized by simply making appropriate changes in the nondimensionalizing parameters. The stability derivatives C_{L_q} and C_{m_q} are available in reference 1 for subsonic leading edges and in reference 3 for supersonic leading edges. At present there is no information for the zero-end-plate solution corresponding to the subsonic-leading-edge condition; for supersonic leading edges the following expressions have been obtained:

$$B(C_{Y_r})_{t,0} = \frac{-2\left(\frac{bvt}{b}\right)^3 KBC}{3A_{r,t}^2(1-K)(KBC-1)^2(B^2C^2-1)\sqrt{K(BC+1)}\sqrt{K(BC-1)}} \left[\epsilon K^2 B^4 C^4 (-1+2K) + \right. \\ \left. 4KB^3C^3(4-9K+K^2) + 4B^2C^2(-2+\epsilon K+K^2-5K^3) + \right. \\ \left. 4BC(-1-5K+10K^2) + 4(3-5K) \right] \quad (19)$$

$$B(C_{n_r})_{t,o} = \frac{2A\left(\frac{b_{vt}}{b}\right)^4 KBC}{15A_{vt}^3(1-K)^2(KBC-1)^3(B^2C^2-1)\sqrt{K(BC+1)}\sqrt{K(BC-1)}} \left[40K^3B^5C^5(-1+3K-3K^2) + \right. \\ \left. 2K^2B^4C^4(61-193K+213K^2-21K^3) + KB^3C^3(-112+403K- \right. \\ \left. 472K^2-37K^3+138K^4) + B^2C^2(30-152K+89K^2+390K^3- \right. \\ \left. 449K^4+12K^5) + BC(15+122K-441K^2+436K^3-12K^4) + \right. \\ \left. (-45+130K-125K^2) \right] \quad (20)$$

Equations (19) and (20) are applicable to sweptback vertical tails of arbitrary aspect ratio and zero taper ratio with supersonic leading and trailing edges; rotation and moments are measured about the apex of the vertical tail.

The differences between the two methods of estimating the tail contribution to the yawing derivatives may be evaluated. Figure 21 presents the results for $(C_{Y_r})_t$ based on equation (16) and also the limiting

cases corresponding to zero- and complete-end-plate situations using equation (19) and wing results for C_{L_q} . (The numerical results presented in figure 21 are for a yawing motion about the center of gravity; hence the usual transfer-of-axis formula, which involves the previously mentioned $(C_{Y_\beta})_{t,o}$, must be used in conjunction with equation (19).)

It is seen that an average value for $(C_{Y_r})_t$ based on the second method would not be significantly different from the value calculated by equation (16). A similar situation was found to exist for the derivative $(C_{n_r})_t$. In view of this evidence, it was not felt necessary to estimate the zero- and complete-end-plate solutions for $(C_{l_r})_t$. Thus equation (18) was used to calculate the tail contribution to C_{l_r} .

With regard to the body contribution to the side force and yawing moment, the difficulties previously encountered for sideslip motion are also present for the yawing motion. These have been treated in an analagous manner (see sideslip section) using equivalent bodies of revolution and results obtainable in references 15 and 16. The body contribution to the rolling moment was assumed to be small and hence was neglected.

The derivatives C_{Y_r} , C_{n_r} , and C_{l_r} for the complete configuration (and for the body and tail contributions) are presented in figures 22, 23, and 24, respectively.

CONCLUDING REMARKS

Theoretical calculations of the stability derivatives at supersonic speeds for a high-speed airplane configuration have been presented. The methods used represent detailed consideration of the important effects and contributions of the various airplane components utilizing available theories and theoretically justifiable and reasonable approximations. The results are valid for motions involving small angles of attack and sideslip and low rates of rolling, pitching, and yawing.

It should be emphasized that the theoretical information available, although supplying many of the basic requirements, is by no means sufficient to allow estimation of the various forces, moments, and stability derivatives for arbitrary complete configurations. Some of the approximations developed in the present analysis would be applicable; others would require considerable modifications depending on the configuration under study. It is felt, however, that a detailed analysis analagous to that undertaken for the present airplane would result in reliable estimates for many types of complete airplane configurations suitable for supersonic flight. Further theoretical research on fundamental problems indicated in the text is of course required in order to improve the accuracy of the estimations and to help minimize the time and effort required to obtain them.

Langley Aeronautical Laboratory,
National Advisory Committee for Aeronautics,
Langley Field, Va., July 27, 1953.

REFERENCES

1. Malvestuto, Frank S., Jr., and Margolis, Kenneth: Theoretical Stability Derivatives of Thin Sweptback Wings Tapered to a Point With Sweptback or Sweptforward Trailing Edges for a Limited Range of Supersonic Speeds. NACA Rep. 971, 1950. (Supersedes NACA TN 1761.)
2. Harmon, Sidney M., and Jeffreys, Isabella: Theoretical Lift and Damping in Roll of Thin Wings With Arbitrary Sweep and Taper at Supersonic Speeds. Supersonic Leading and Trailing Edges. NACA TN 2114, 1950.
3. Martin, John C., Margolis, Kenneth, and Jeffreys, Isabella: Calculation of Lift and Pitching Moments Due to Angle of Attack and Steady Pitching Velocity at Supersonic Speeds for Thin Sweptback Tapered Wings With Streamwise Tips and Supersonic Leading and Trailing Edges. NACA TN 2699, 1952.
4. Nielson, Jack N., and Kaattari, George E.: Method for Estimating Lift Interference of Wing-Body Combinations at Supersonic Speeds. NACA RM A51J04, 1951.
5. Kaattari, George E., Nielson, Jack N., and Pitts, William C.: Method for Estimating Pitching-Moment Interference of Wing-Body Combinations at Supersonic Speed. NACA RM A52B06, 1952.
6. Tucker, Warren A.: A Method for Estimating the Components of Lift of Wing-Body Combinations at Supersonic Speeds. NACA RM L52D22, 1952.
7. Moskowitz, Barry: Approximate Theory for Calculations of Lift of Bodies, Afterbodies, and Combinations of Bodies. NACA TN 2669, 1952.
8. Nonweiler, T.: The Theoretical Lift and Pitching Moment of a Highly-Swept Delta Wing on a Body of Elliptic Cross-Section. Tech. No. Aero. 2055, British R.A.E., June 1950.
9. Mirels, Harold, and Haefeli, Rudolph C.: Line-Vortex Theory for Calculation of Supersonic Downwash. NACA Rep. 983, 1950. (Supersedes NACA TN 1925.)
10. Lomax, Harvard, Sluder, Loma, and Heaslet, Max. A.: The Calculation of Downwash Behind Supersonic Wings With an Application to Triangular Plan Forms. NACA Rep. 957, 1950.

11. Lagerstrom, P. A., Graham, Martha E., and Grosslight, G.: Downwash and Sidewash Induced by Three-Dimensional Lifting Wings in Supersonic Flow. Rep. No. SM-13007, Douglas Aircraft Co., Inc., Apr. 14, 1947.
12. Haefeli, Rudolph C., Mirels, Harold, and Cummings, John L.: Charts for Estimating Downwash Behind Rectangular, Trapezoidal, and Triangular Wings at Supersonic Speeds. NACA TN 2141, 1950.
13. Walker, Harold J., and Ballantyne, Mary B.: Pressure Distribution and Damping in Steady Pitch at Supersonic Mach Numbers of Flat Swept-Back Wings Having all Edges Subsonic. NACA TN 2197, 1950.
14. Miles, John W.: On Damping in Pitch for Delta Wings. Jour. Aero. Sci. (Readers' Forum), vol. 16, no. 9, Sept. 1949, pp. 574-575.
15. Smith, C. B., and Beane, Beverly J.: Damping in Pitch of Bodies of Revolution at Supersonic Speeds. Preprint No. 311, Inst. Aero. Sci., Feb. 1951.
16. Dorrance, William H.: Nonsteady Supersonic Flow About Pointed Bodies of Revolution. Jour. Aero. Sci., vol. 18, no. 8, Aug. 1951, pp. 505-511, 542.
17. Ribner, Herbert S.: Time-Dependent Downwash at the Tail and the Pitching Moment Due to Normal Acceleration at Supersonic Speeds. NACA TN 2042, 1950.
18. Henderson, Arthur, Jr.: Pitching-Moment Derivatives C_{mq} and $C_{m\dot{\alpha}}$ at Supersonic Speeds for a Slender-Delta-Wing and Slender-Body Combination and Approximate Solutions for Broad-Delta-Wing and Slender-Body Combinations. NACA TN 2553, 1951.
19. Margolis, Kenneth: Theoretical Calculations of the Lateral Force and Yawing Moment Due to Rolling at Supersonic Speeds for Swept-back Tapered Wings With Streamwise Tips. Subsonic Leading Edges. NACA TN 2122, 1950.
20. Harmon, Sidney M., and Martin, John C.: Theoretical Calculations of the Lateral Force and Yawing Moment Due to Rolling at Supersonic Speeds for Sweptback Tapered Wings With Streamwise Tips. Supersonic Leading Edges. NACA TN 2156, 1950.
21. Malvestuto, Frank S., Jr., Margolis, Kenneth, and Ribner, Herbert S.: Theoretical Lift and Damping in Roll at Supersonic Speeds of Thin Sweptback Tapered Wings With Streamwise Tips, Subsonic Leading Edges, and Supersonic Trailing Edges. NACA Rep. 970, 1950. (Supersedes NACA TN 1860.)

22. Margolis, Kenneth: Theoretical Lift and Damping in Roll of Thin Sweptback Tapered Wings With Raked-In and Cross-Stream Wing Tips at Supersonic Speeds. Subsonic Leading Edges. NACA TN 2048, 1950.
23. Walker, Harold J., and Ballantyne, Mary B.: Pressure Distribution and Damping in Steady Roll at Supersonic Mach Numbers of Flat Swept-Back Wings With Subsonic Edges. NACA TN 2047, 1950.
24. Bleviss, Zemun O.: Some Roll Characteristics of Cruciform Delta Wings at Supersonic Speeds. Jour. Aero. Sci., vol. 18, no. 5, May 1951, pp. 289-297.
25. Tucker, Warren A., and Piland, Robert O.: Estimation of the Damping in Roll of Supersonic-Leading-Edge Wing-Body Combinations. NACA TN 2151, 1950.
26. Lomax, Harvard, and Heaslet, Max. A.: Damping-In-Roll Calculations for Slender Swept-Back Wings and Slender Wing-Body Combinations. NACA TN 1950, 1949.
27. Ribner, Herbert S.: Damping in Roll of Cruciform and Some Related Delta Wings at Supersonic Speeds. NACA TN 2285, 1951.
28. Bobbitt, Percy J., and Malvestuto, Frank S., Jr.: Estimation of Forces and Moments Due to Rolling for Several Slender-Tail Configurations at Supersonic Speeds. NACA TN 2955, 1953.
29. Adams, Gaynor J.: Theoretical Damping in Roll and Rolling Effectiveness of Slender Cruciform Wings. NACA TN 2270, 1951.
30. Scherrer, Richard, and Dennis, David H.: Damping in Roll of a Missile Configuration With a Modified Triangular Wing and a Cruciform Tail at a Mach Number of 1.52. NACA RM A51A03, 1951.
31. Hannah, Margery E., and Margolis, Kenneth: Span Load Distributions Resulting From Constant Angle of Attack, Steady Rolling Velocity, Steady Pitching Velocity, and Constant Vertical Acceleration for Tapered Sweptback Wings With Streamwise Tips - Subsonic Leading Edges and Supersonic Trailing Edges. NACA TN 2831, 1952.
32. Martin, John C., and Jeffrey, Isabella: Span Load Distributions Resulting From Angle of Attack, Rolling, and Pitching for Tapered Sweptback Wings With Streamwise Tips. Supersonic Leading and Trailing Edges. NACA TN 2643, 1952.

33. Michael, William H., Jr.: Analysis of the Effects of Wing Interference on the Tail Contributions to the Rolling Derivatives. NACA Rep. 1066, 1952. (Supersedes NACA TN 2332.)
34. Martin, John C.: The Calculation of Downwash Behind Wings of Arbitrary Plan Form at Supersonic Speeds. NACA TN 2135, 1950.
35. Katzoff, S., and Mutterperl, William: The End-Plate Effect of a Horizontal-Tail Surface on a Vertical-Tail Surface. NACA TN 797, 1941.
36. Jones, Arthur L., Spreiter, John R., and Alksne, Alberta: The Rolling Moment Due to Sideslip of Triangular, Trapezoidal, and Related Plan Forms in Supersonic Flow. NACA TN 1700, 1948.
37. Jones, Arthur L., and Alksne, Alberta: The Yawing Moment Due to Sideslip of Triangular, Trapezoidal, and Related Plan Forms in Supersonic Flow. NACA TN 1850, 1949.
38. Margolis, Kenneth, Sherman, Windsor L., and Hannah, Margery E.: Theoretical Calculation of the Pressure Distribution, Span Loading, and Rolling Moment Due to Sideslip at Supersonic Speeds for Thin Sweptback Tapered Wings With Supersonic Trailing Edges and Wing Tips Parallel to the Axis of Wing Symmetry. NACA TN 2898, 1953.
39. Robinson, A., and Hunter-Tod, J. H.: The Aerodynamic Derivatives With Respect to Sideslip for a Delta Wing With Small Dihedral at Supersonic Speeds. Rep. No. 12, College of Aero., Cranfield (British), Dec. 1947.
40. Purser, Paul E.: An Approximation to the Effect of Geometric Dihedral on the Rolling Moment Due to Sideslip for Wings at Transonic and Supersonic Speeds. NACA RM L52B01, 1952.
41. Spreiter, John R.: The Aerodynamic Forces on Slender Plane- and Cruciform-Wing and Body Combinations. NACA Rep. 962, 1950. (Supersedes NACA TN'S 1897 and 1662.)
42. Martin, John C., and Malvestuto, Frank S., Jr.: Theoretical Force and Moments Due to Sideslip of a Number of Vertical Tail Configurations at Supersonic Speeds. NACA TN 2412, 1951.
43. Heaslet, Max. A., Lomax, Harvard, and Jones, Arthur L.: Volterra's Solution of the Wave Equation as Applied to Three-Dimensional Supersonic Airfoil Problems. NACA Rep. 889, 1947. (Supersedes NACA TN 1412.)

44. Ribner, Herbert S.: The Stability Derivatives of Low-Aspect-Ratio Triangular Wings at Subsonic and Supersonic Speeds. NACA TN 1423, 1947.
45. Harmon, Sidney M.: Stability Derivatives at Supersonic Speeds of Thin Rectangular Wings With Diagonals Ahead of Tip Mach Lines. NACA Rep. 925, 1949. (Supersedes NACA TN 1706.)
46. Ribner, Herbert S., and Malvestuto, Frank S., Jr.: Stability Derivatives of Triangular Wings at Supersonic Speeds. NACA Rep. 908, 1948. (Supersedes NACA TN 1572.)

TABLE I.- CHARACTERISTICS OF AIRPLANE CONFIGURATION

[Dimensions correspond to those of a 1/10-scale model]

Over-all length, in.	90
Wing area (total), sq ft	4.01
Wing airfoil section	NACA 65A003
Horizontal-tail area (total), sq ft	0.908
Horizontal-tail airfoil section	NACA 65A003
Vertical-tail area (exposed), sq ft	0.874
Vertical-tail airfoil section	NACA 65A003
Center-of-gravity location, percent M.A.C.	32

The NACA logo, consisting of the word "NACA" in a stylized font with a wing-like shape above and below it.

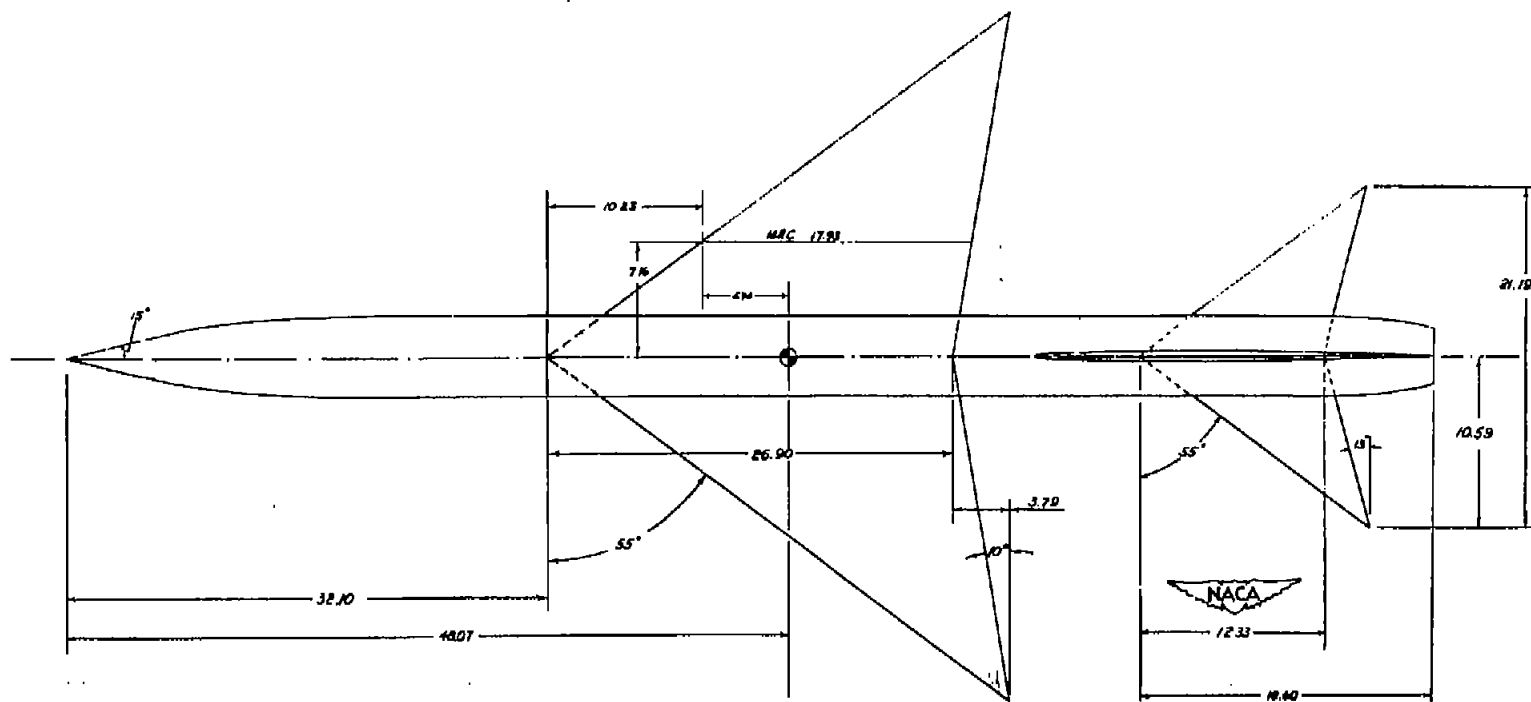


Figure 1.- Geometry and dimensions of configuration. Dimensions shown are in inches and are 1/10-full-scale.

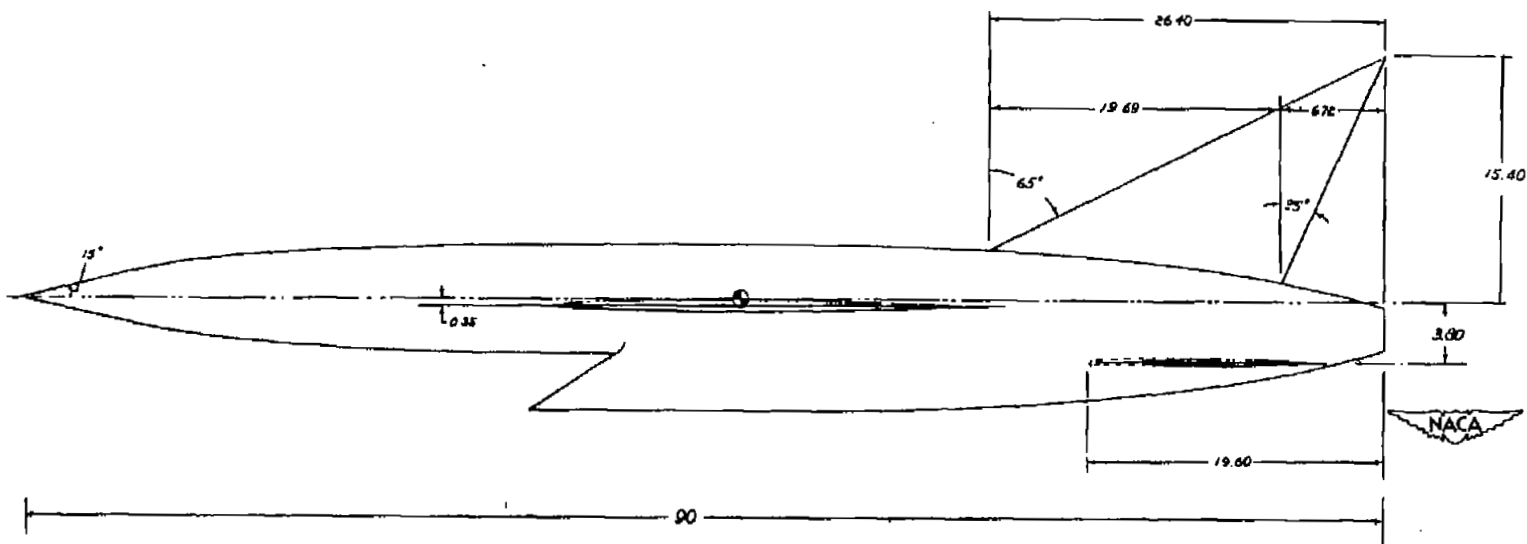


Figure 1.- Continued.

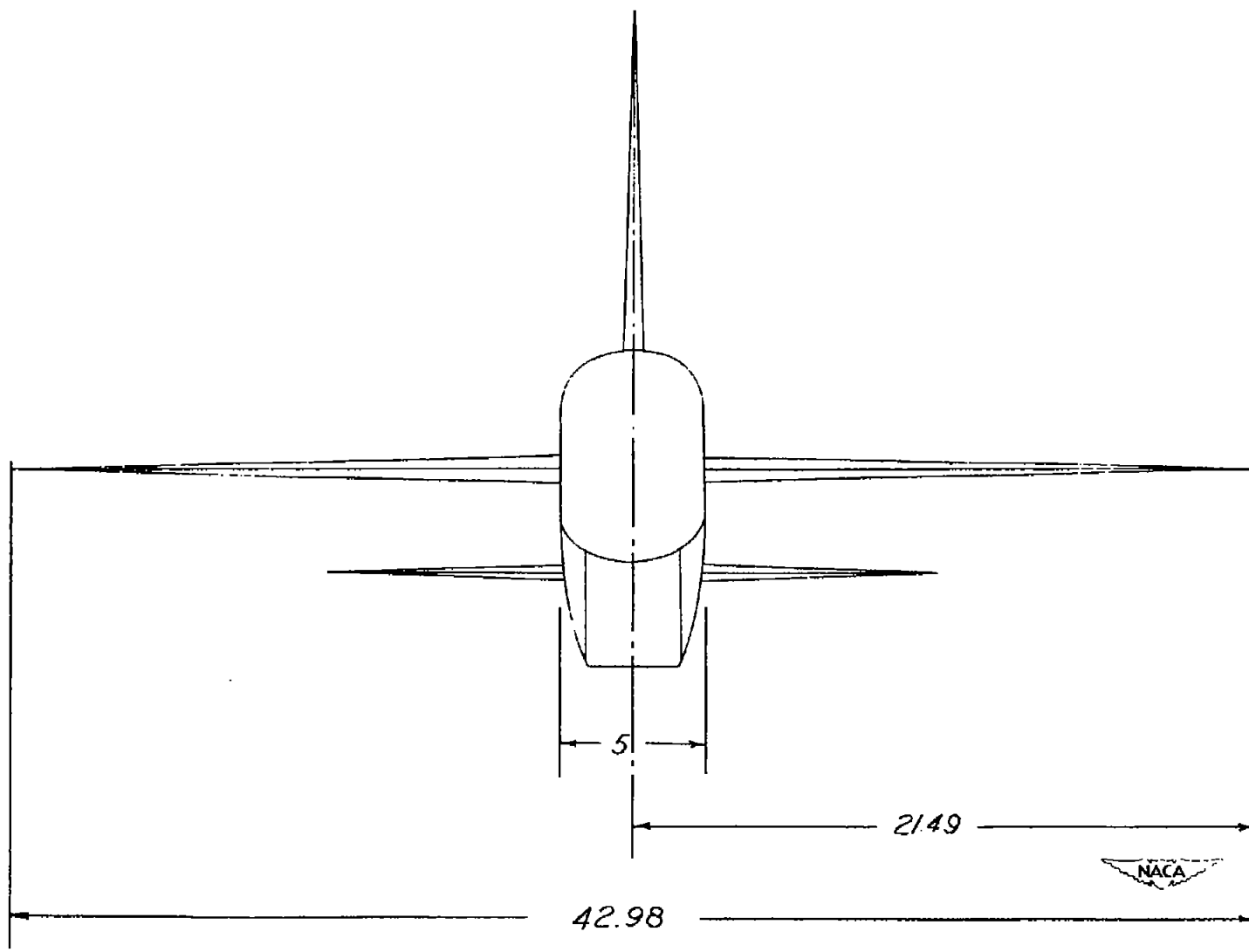


Figure 1.- Concluded.

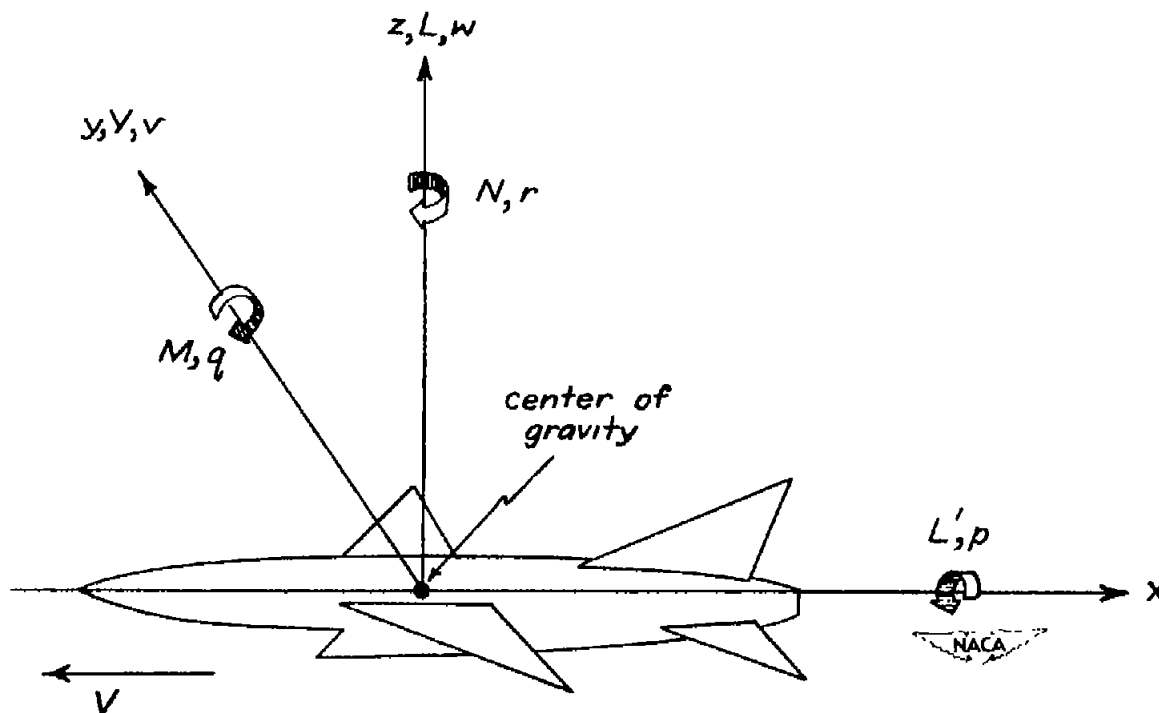


Figure 2.- System of axes, forces, moments, and velocities. (Positive directions indicated by arrows.)

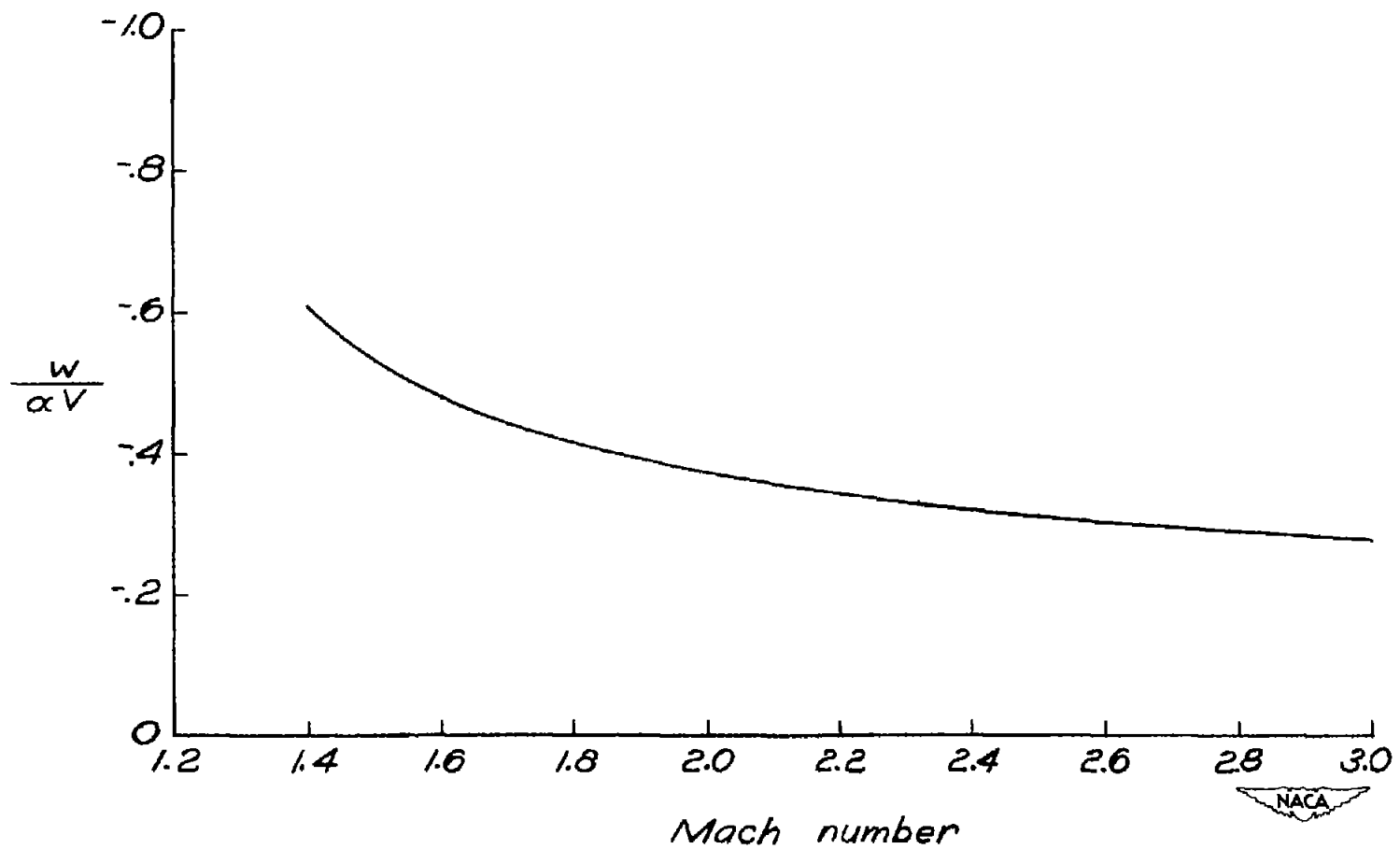


Figure 3.- Variation of the average downwash velocity on the horizontal tail with Mach number. Note that negative values for w denote downwash.

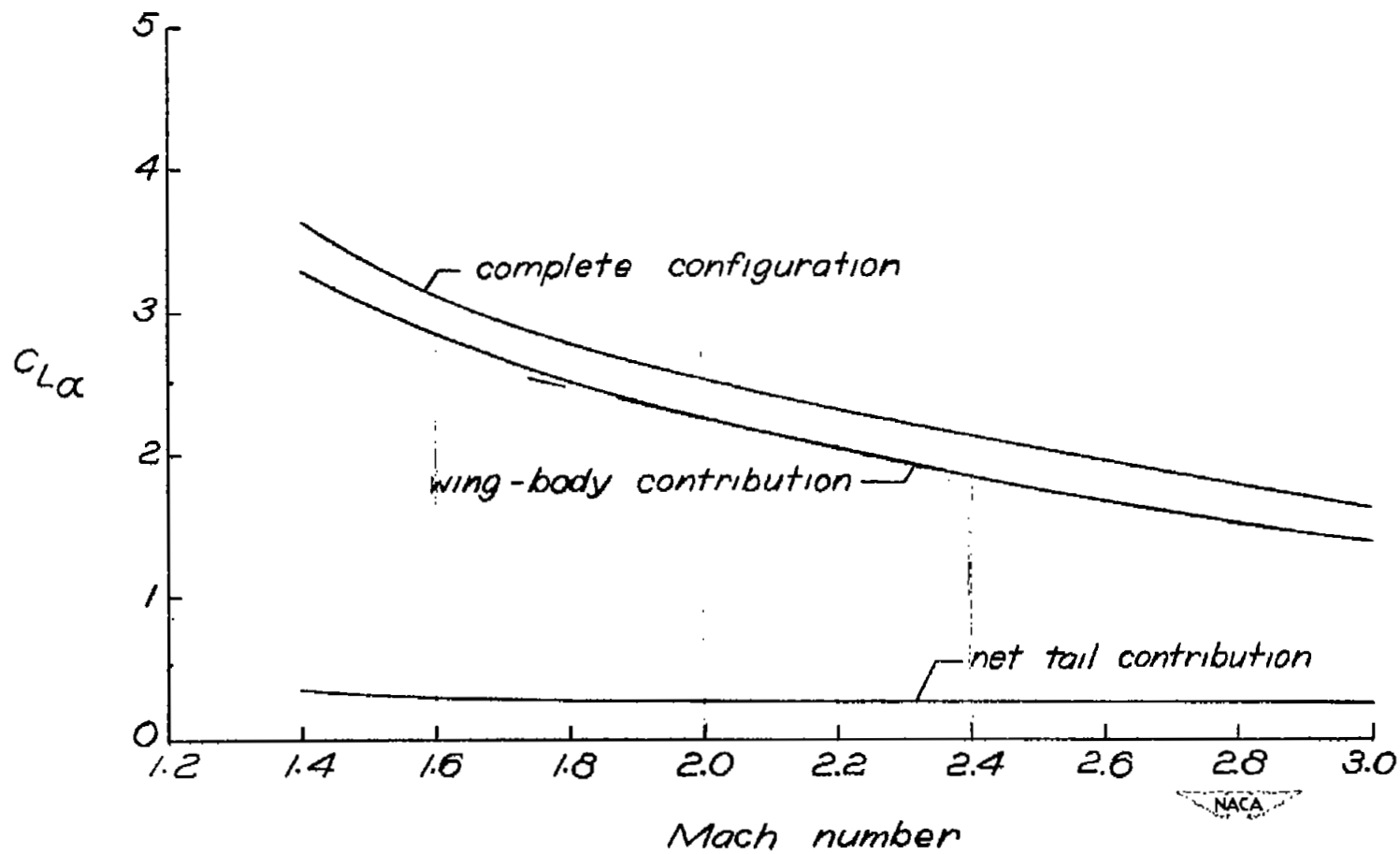


Figure 4.- Variation of the lift-curve slope $C_{L\alpha}$ with Mach number.

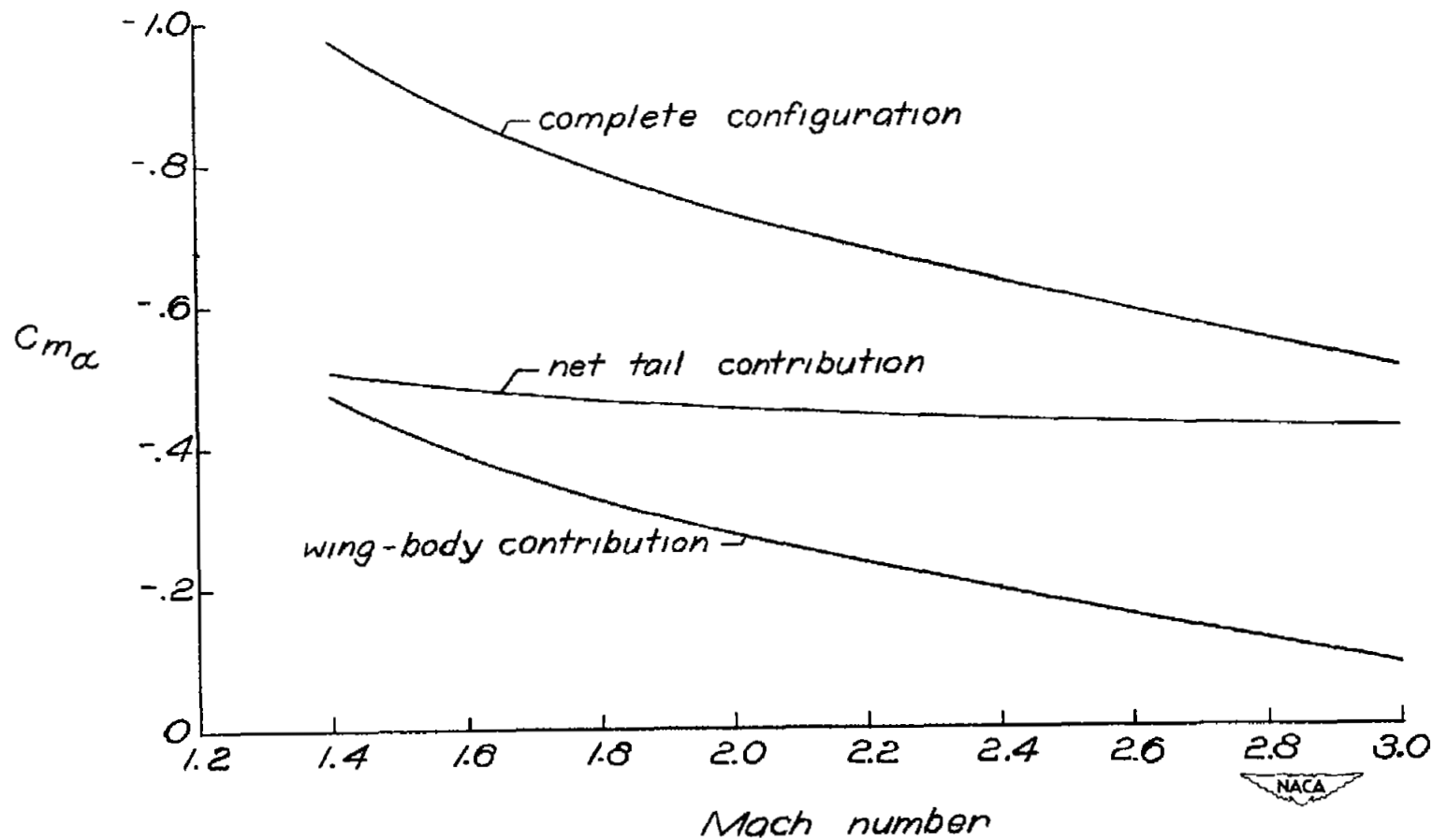


Figure 5.- Variation of the stability derivative $C_{m\alpha}$ with Mach number.

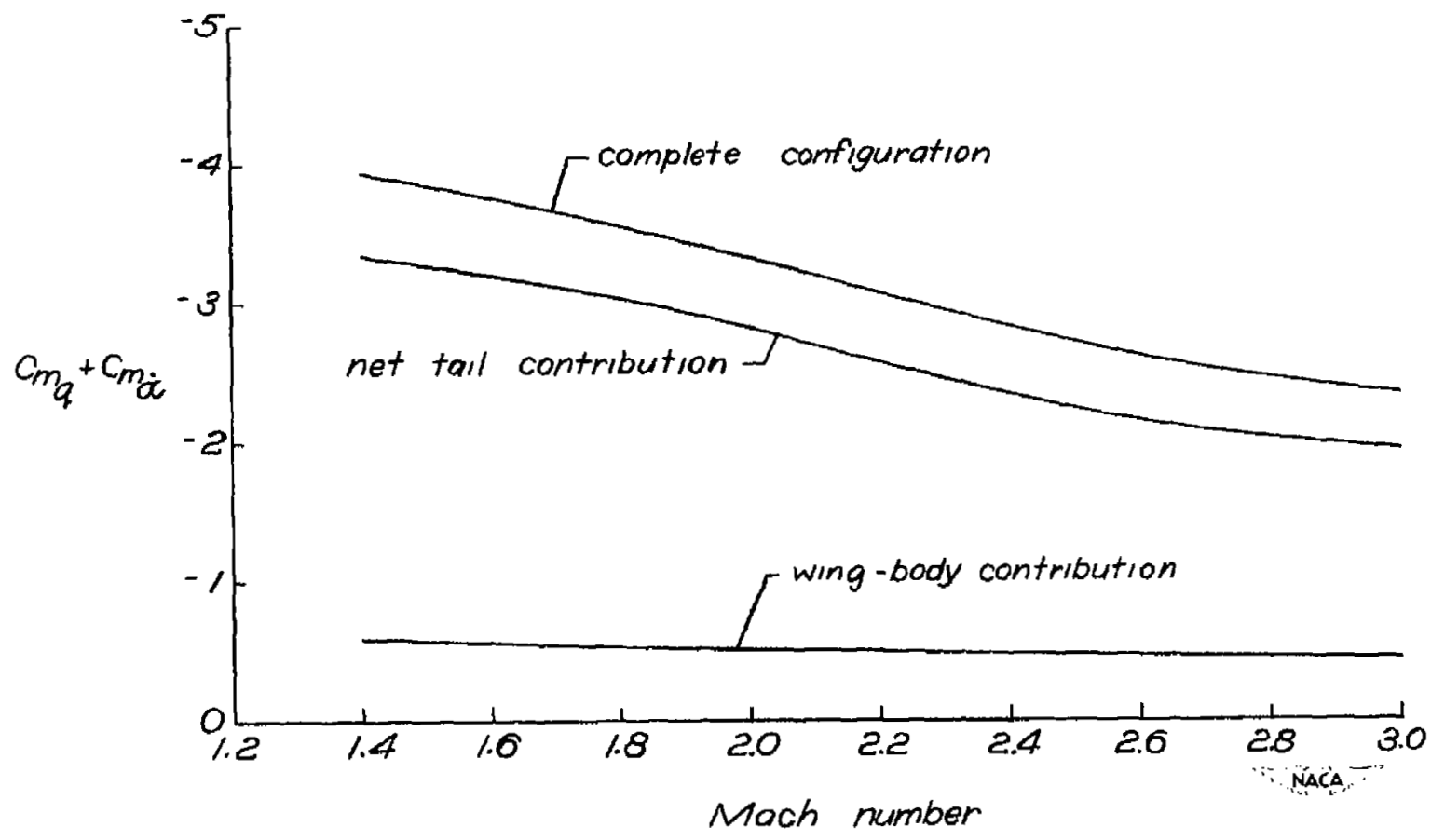


Figure 6.- Variation of the damping in pitch $C_{m_q} + C_{m_{\dot{\alpha}}}$ with Mach number.

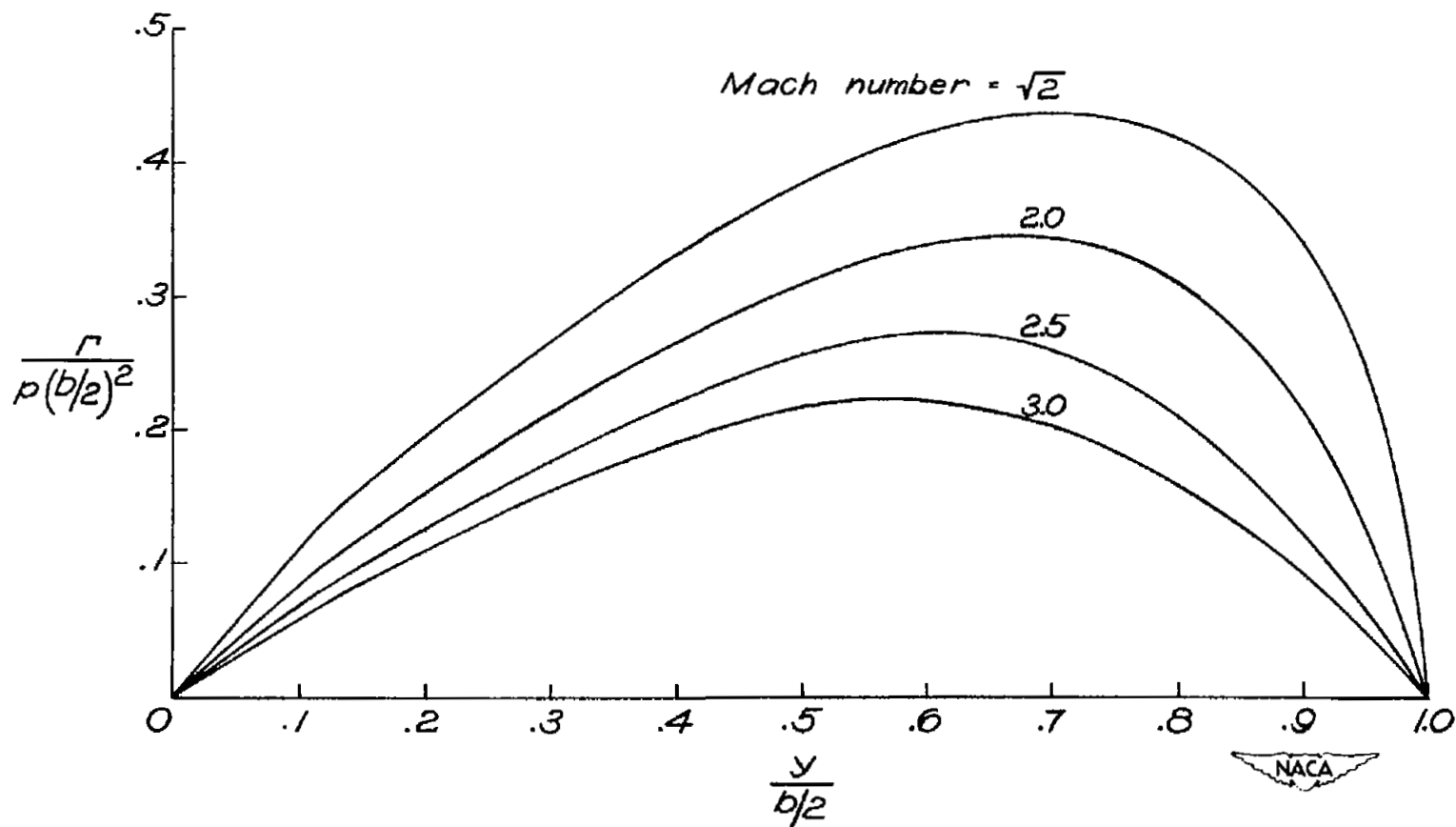


Figure 7.- Span load distributions for the rolling wing-body combination.

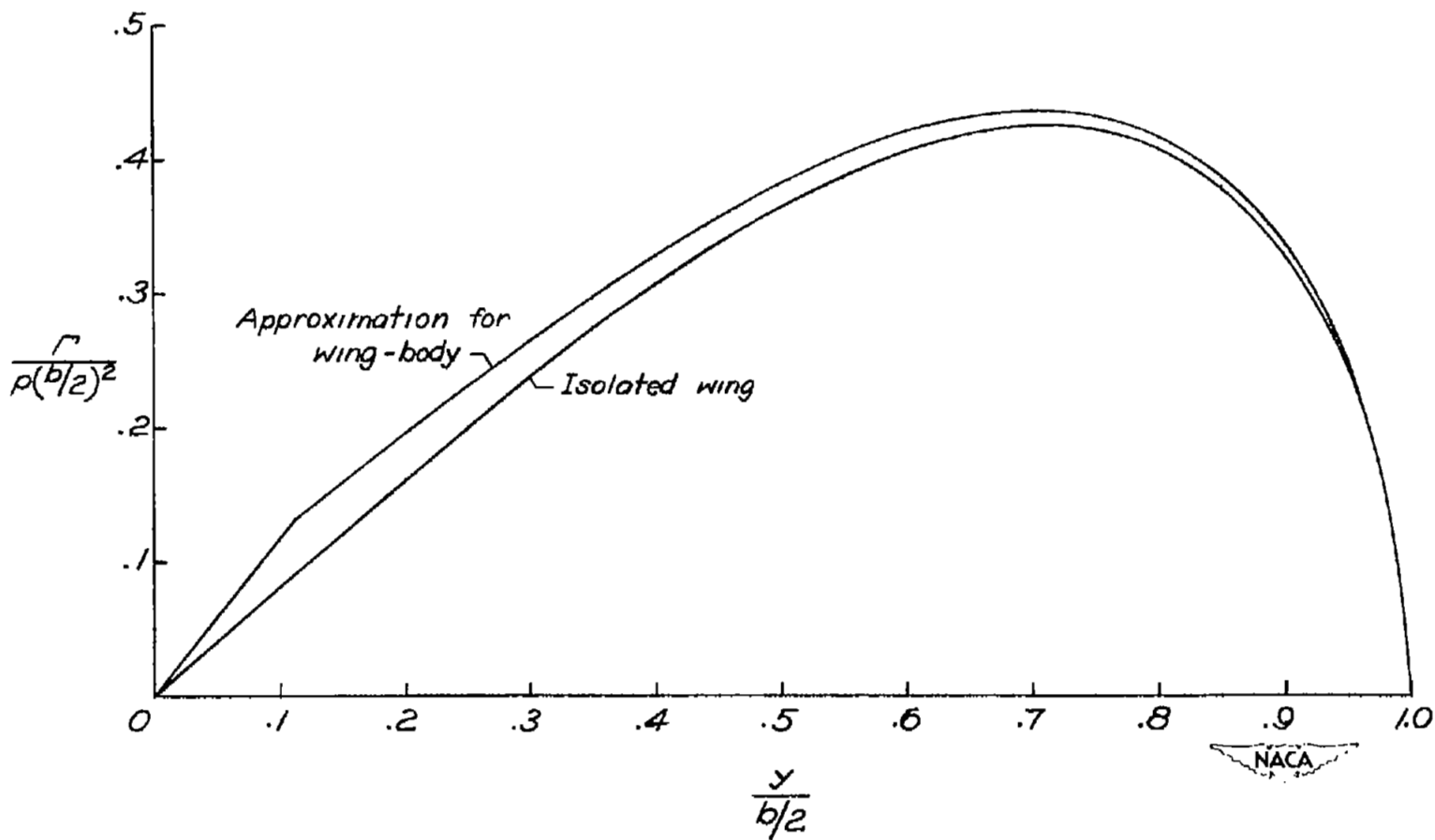


Figure 8.- Comparison at Mach number $\sqrt{2}$ between the span load distributions for the rolling wing-body combination and the corresponding isolated wing.

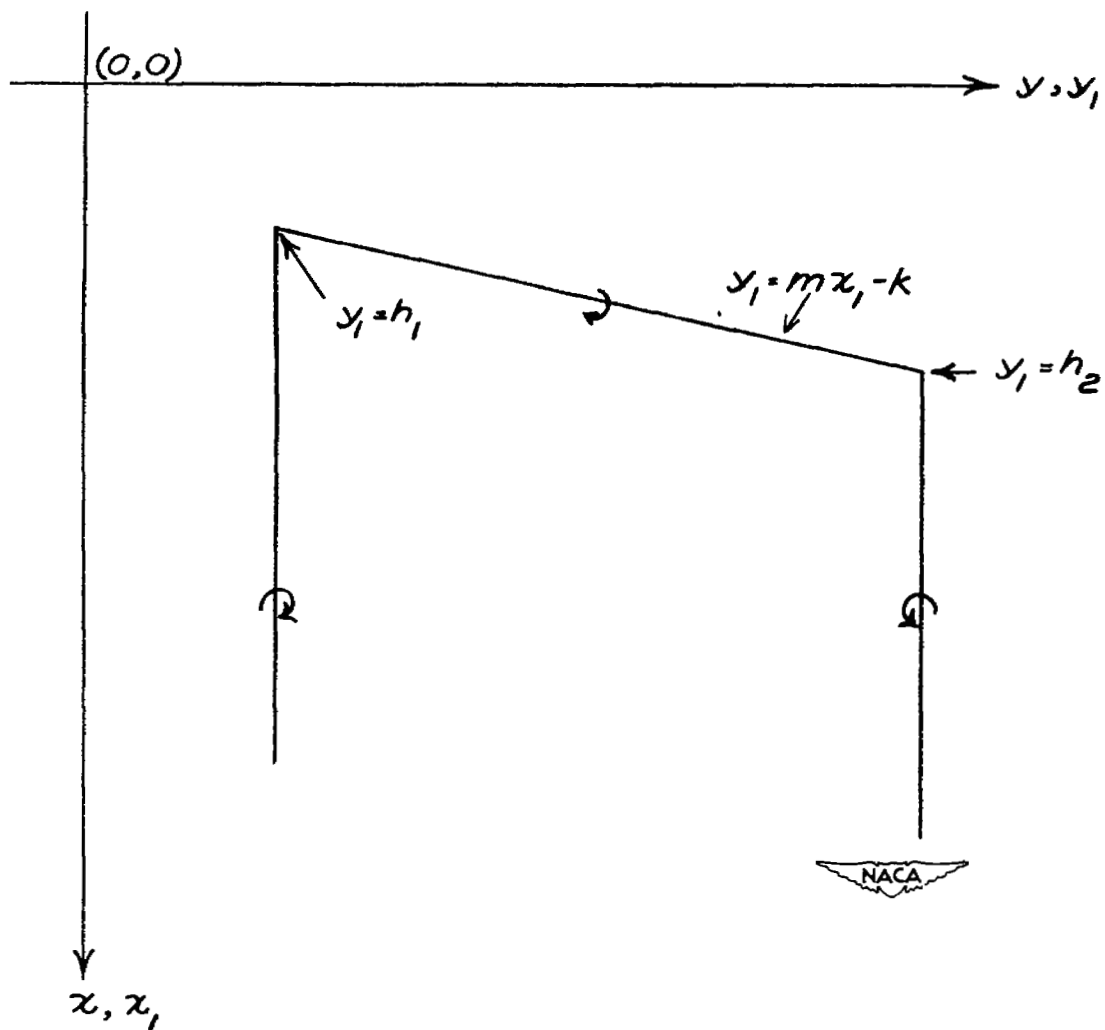


Figure 9.- Finite vortex used to approximate a bent lifting line.

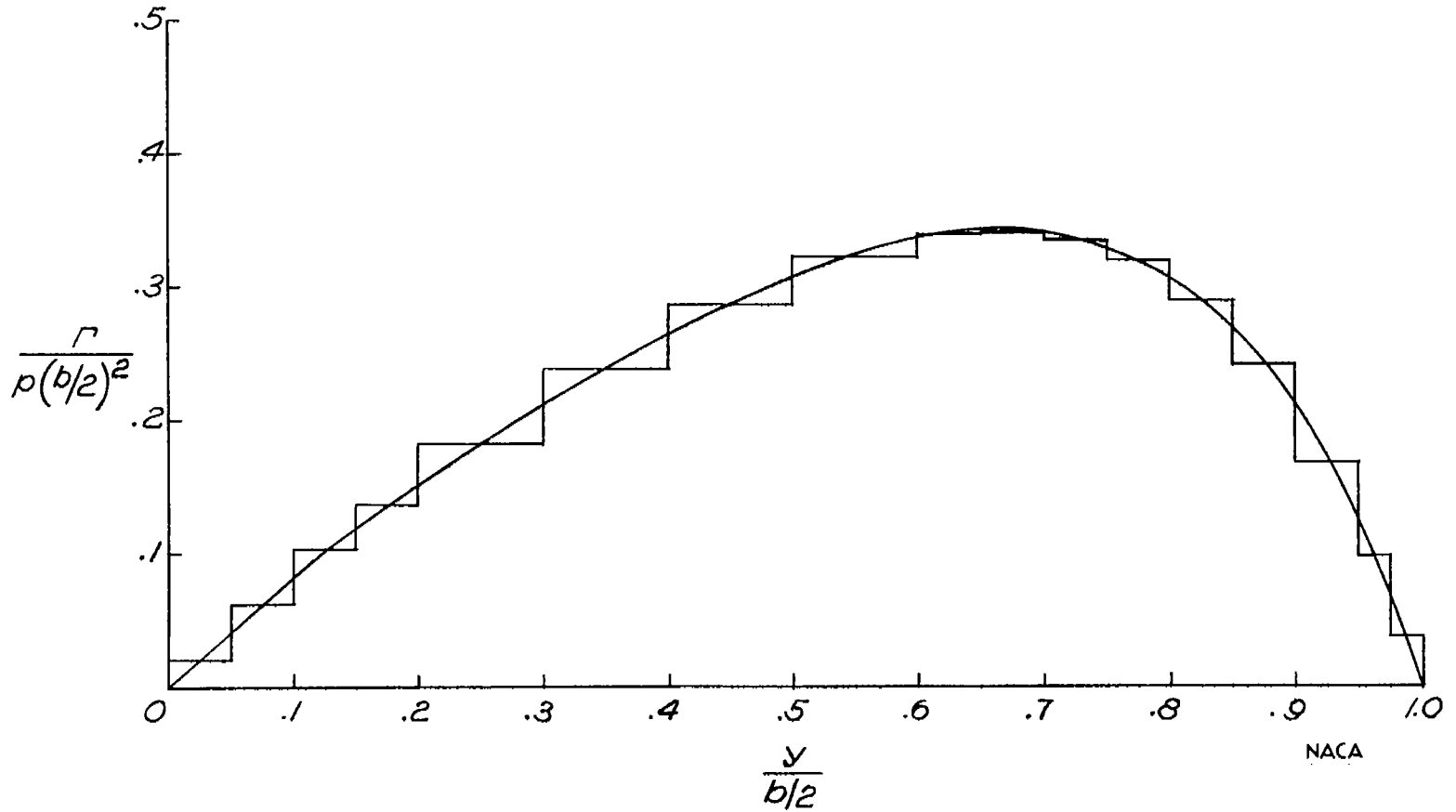


Figure 10.- Approximation of the span loading at Mach number 2.0 for the rolling wing-body combination by superposition of a number of finite-strength vortices.

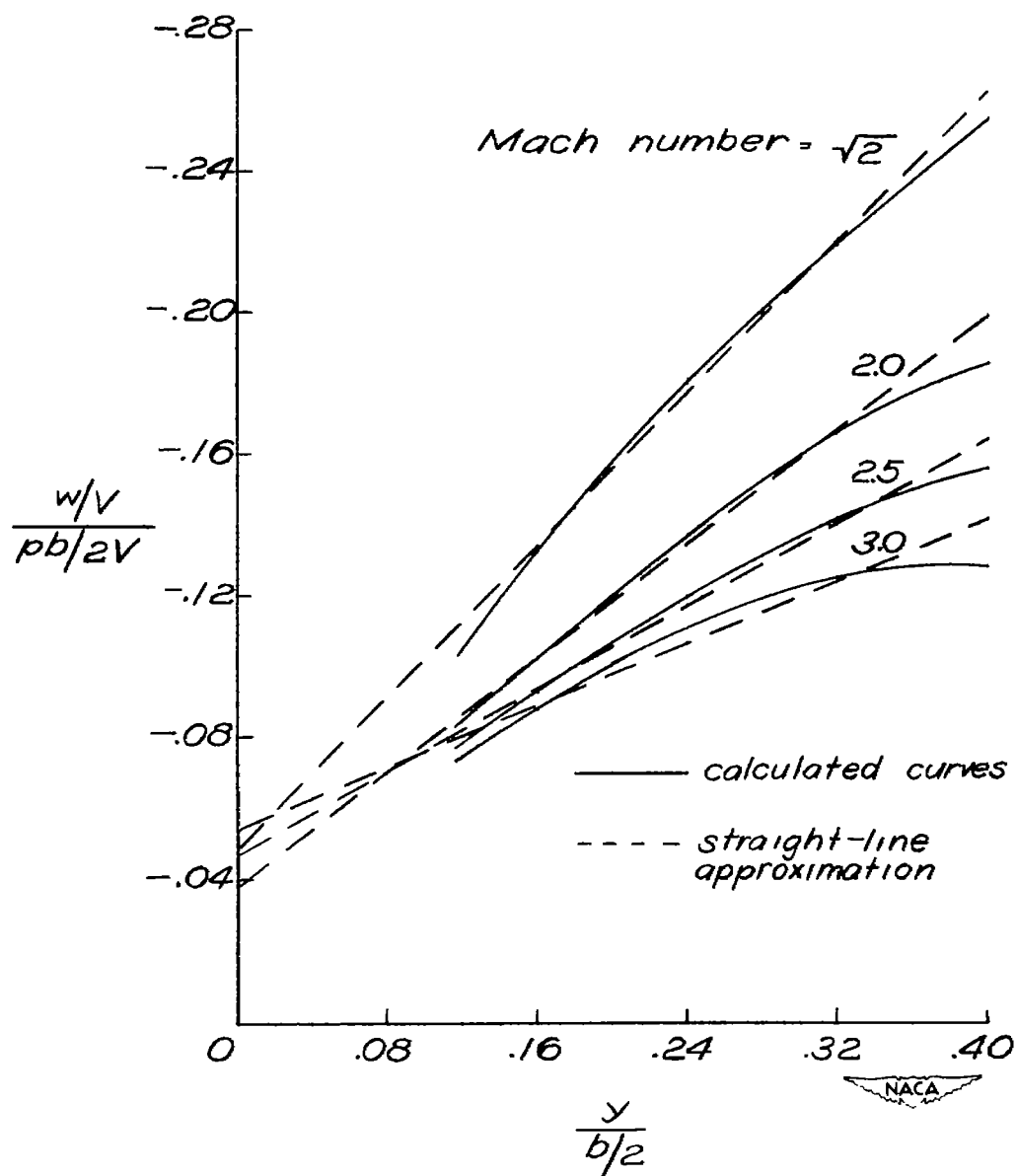


Figure 11.- Induced downwash distributions on the horizontal tail for rolling motion. Note that negative values for w denote downwash.

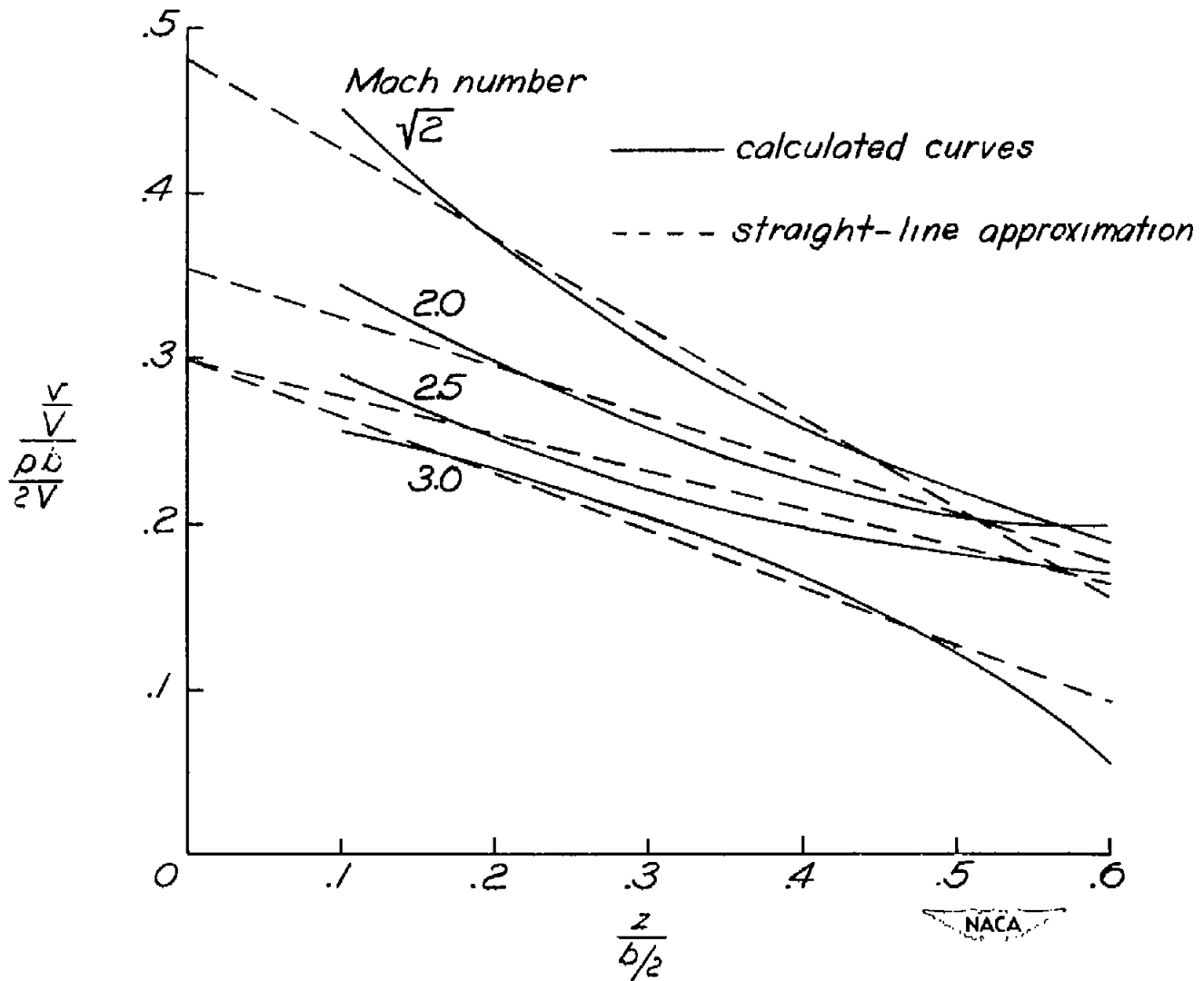


Figure 12.- Induced sidewash distribution on the vertical tail for rolling motion.

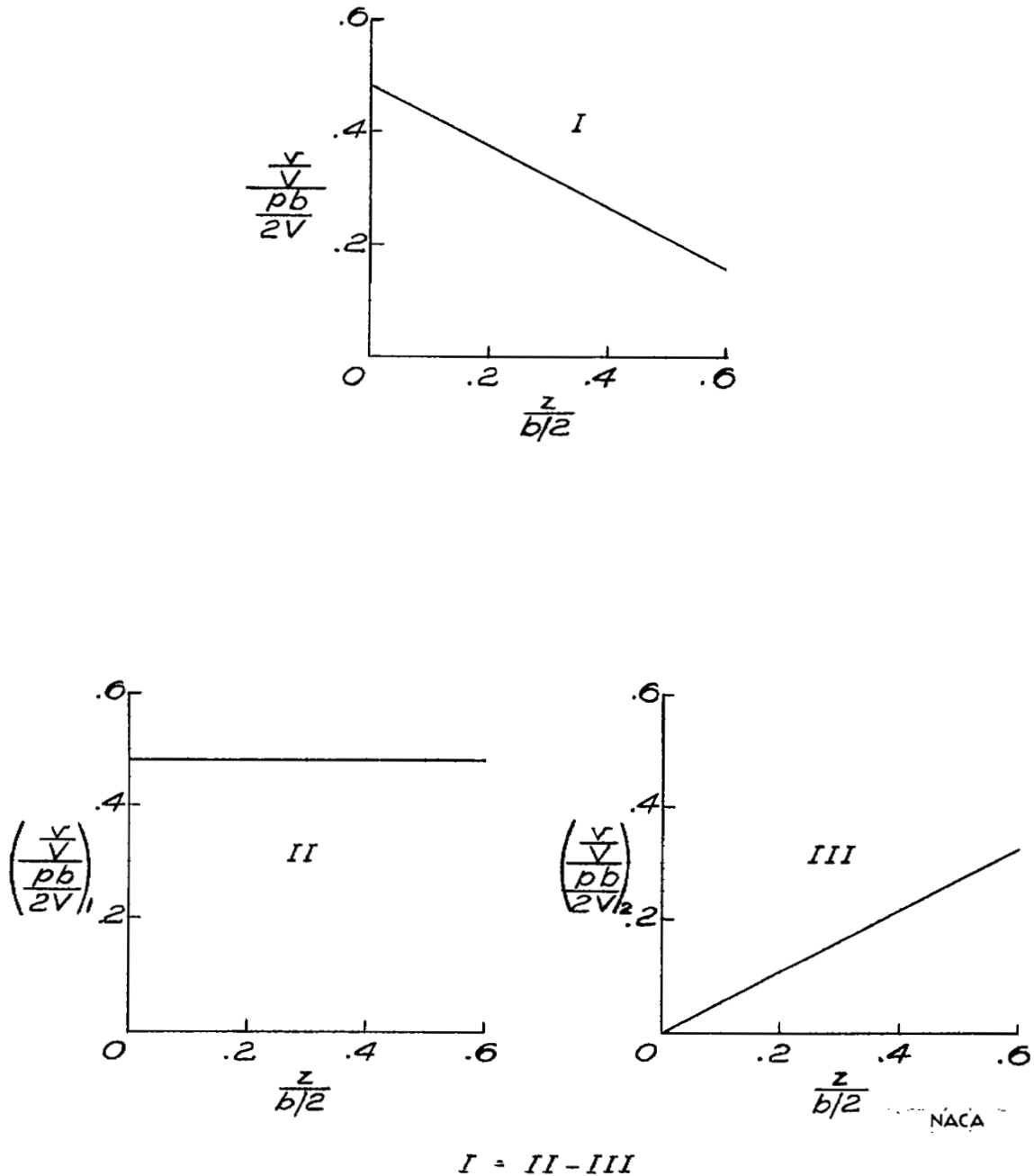


Figure 13.- Procedure used to simulate the induced sidewash (and downwash) distributions by means of superposing elementary solutions.

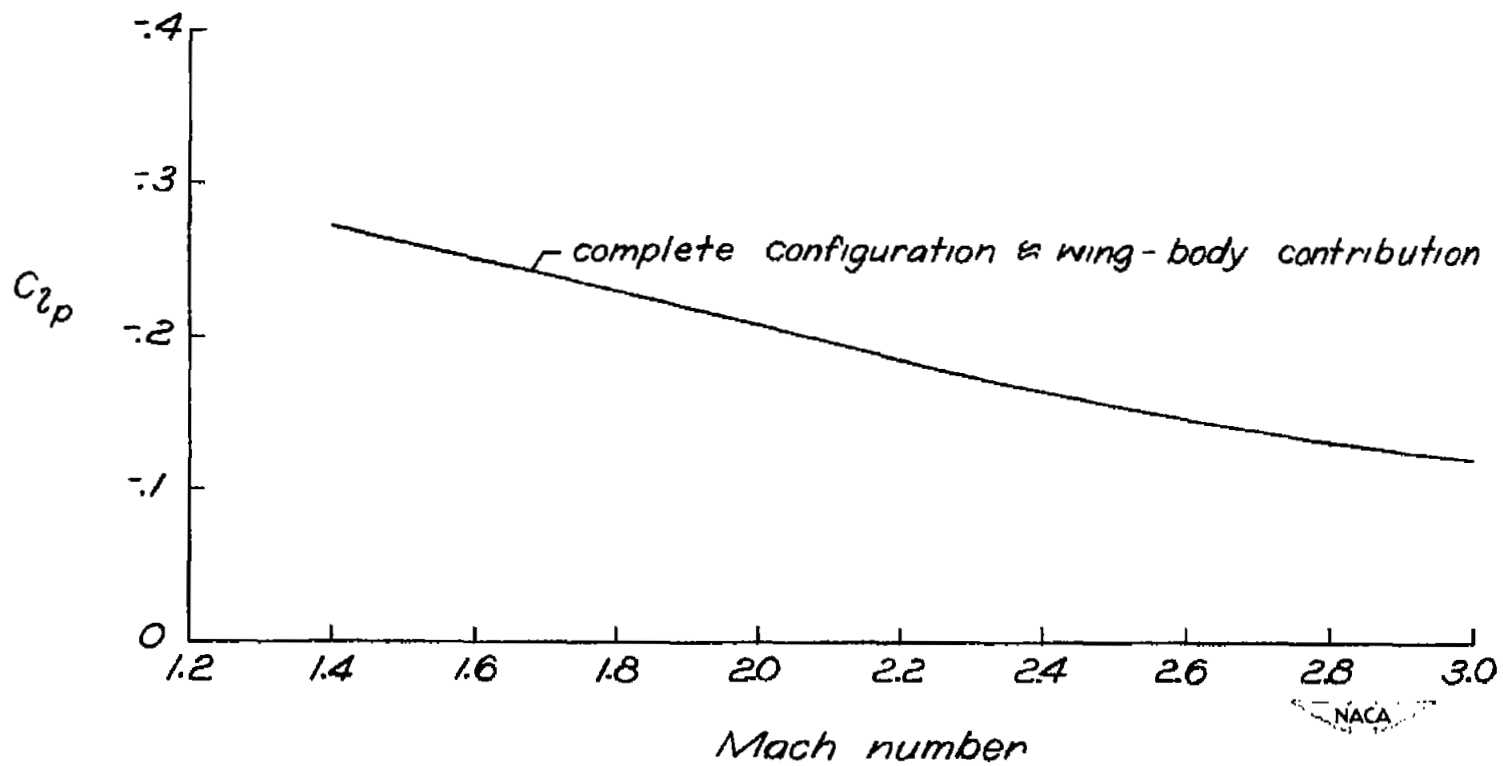


Figure 14.- Variation of the damping in roll C_{lp} with Mach number.

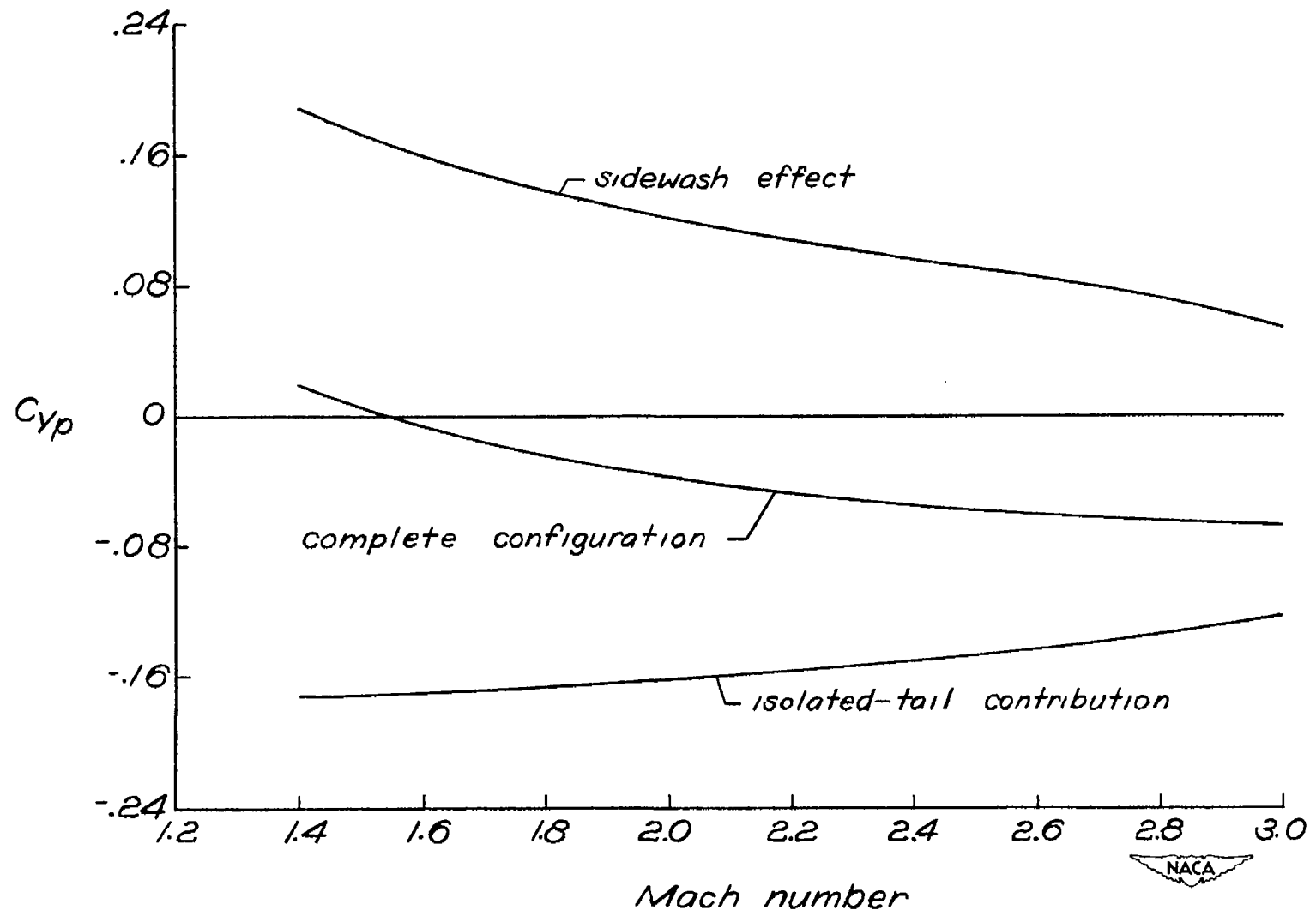


Figure 15.- Variation of the stability derivative C_{yp} with Mach number.

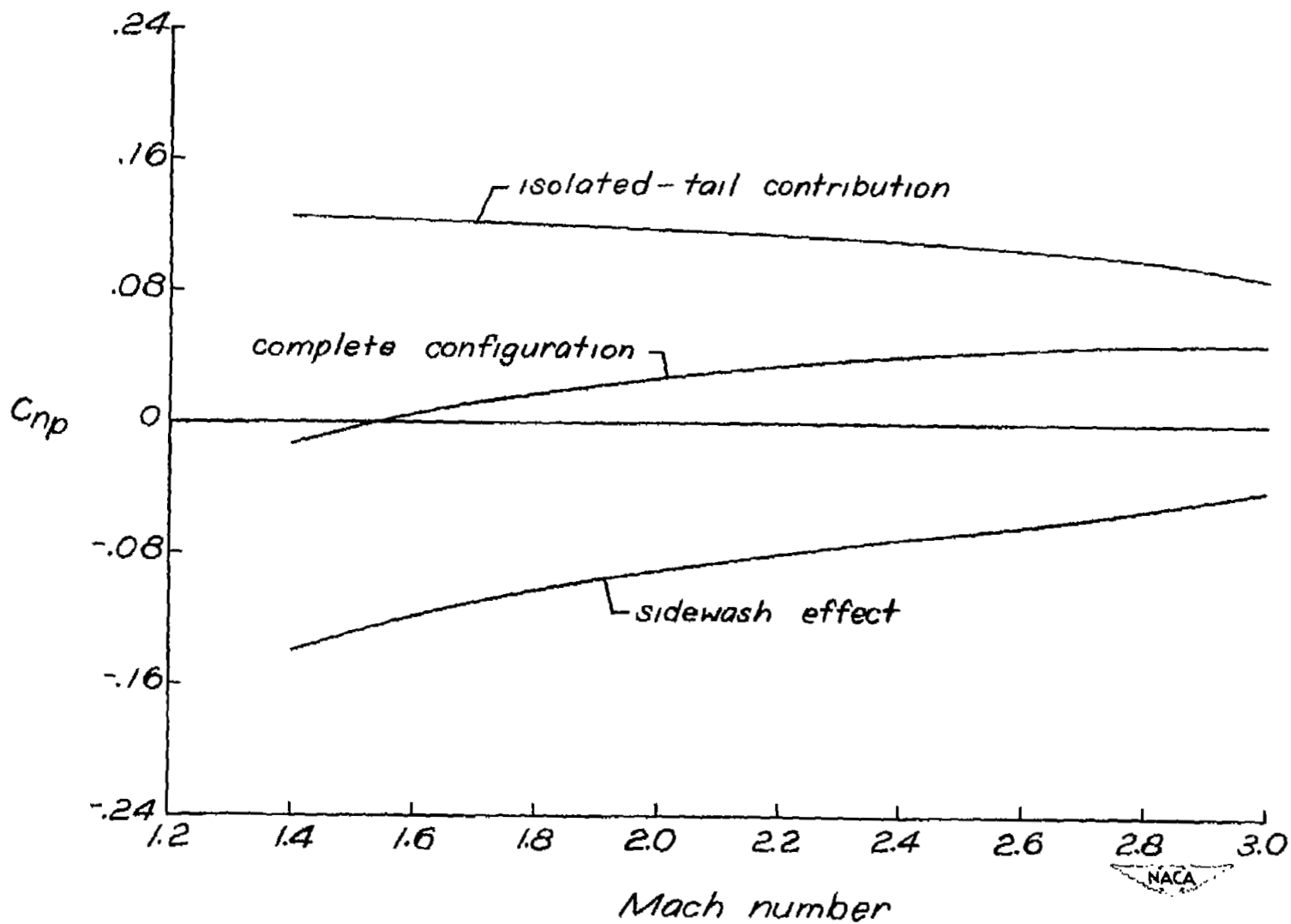


Figure 16.- Variation of the stability derivative C_{np} with Mach number.

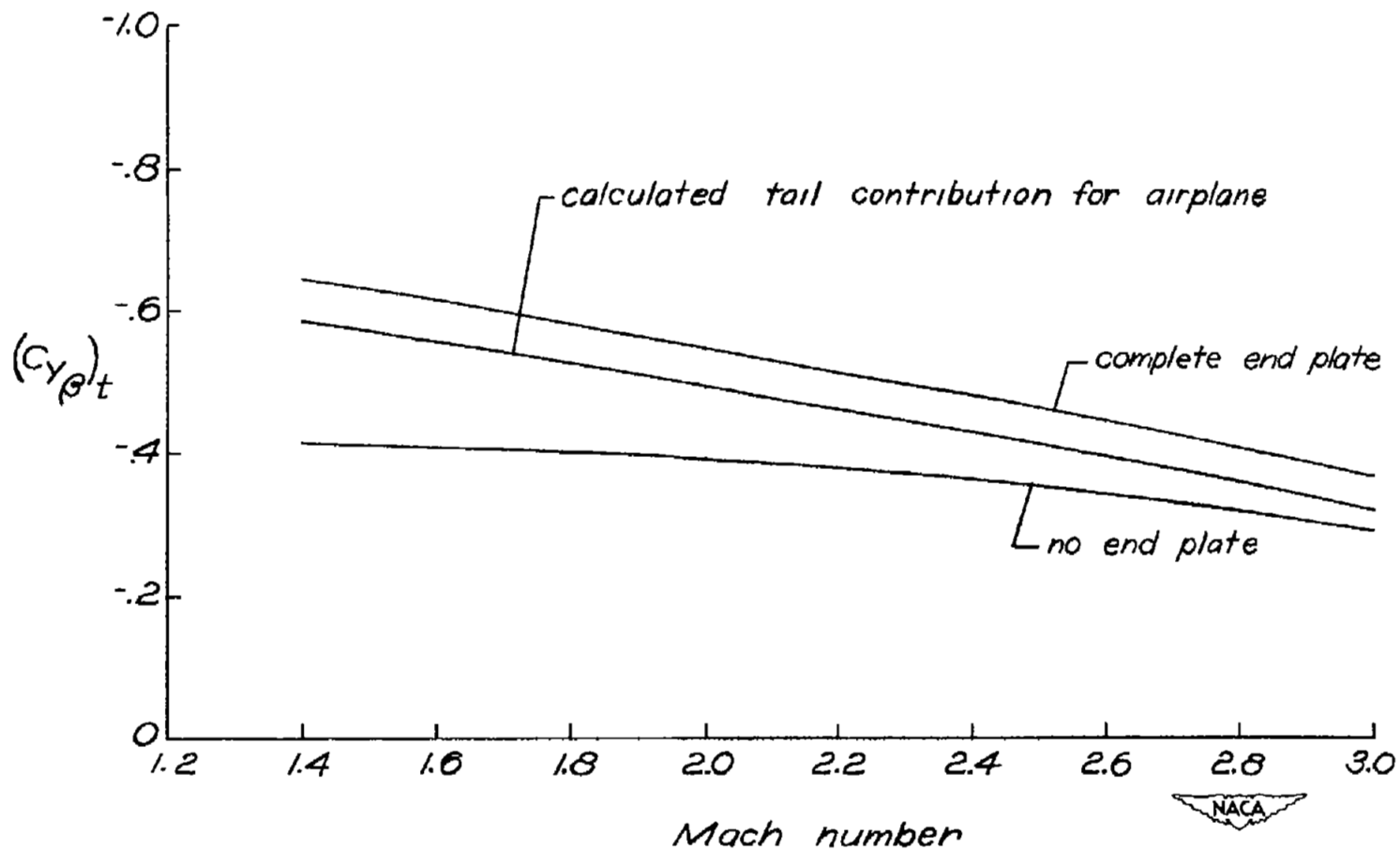


Figure 17.- Comparison of the calculated tail contribution to the stability derivative $C_{Y_{\beta}}$ with the complete- and no-end-plate solutions.

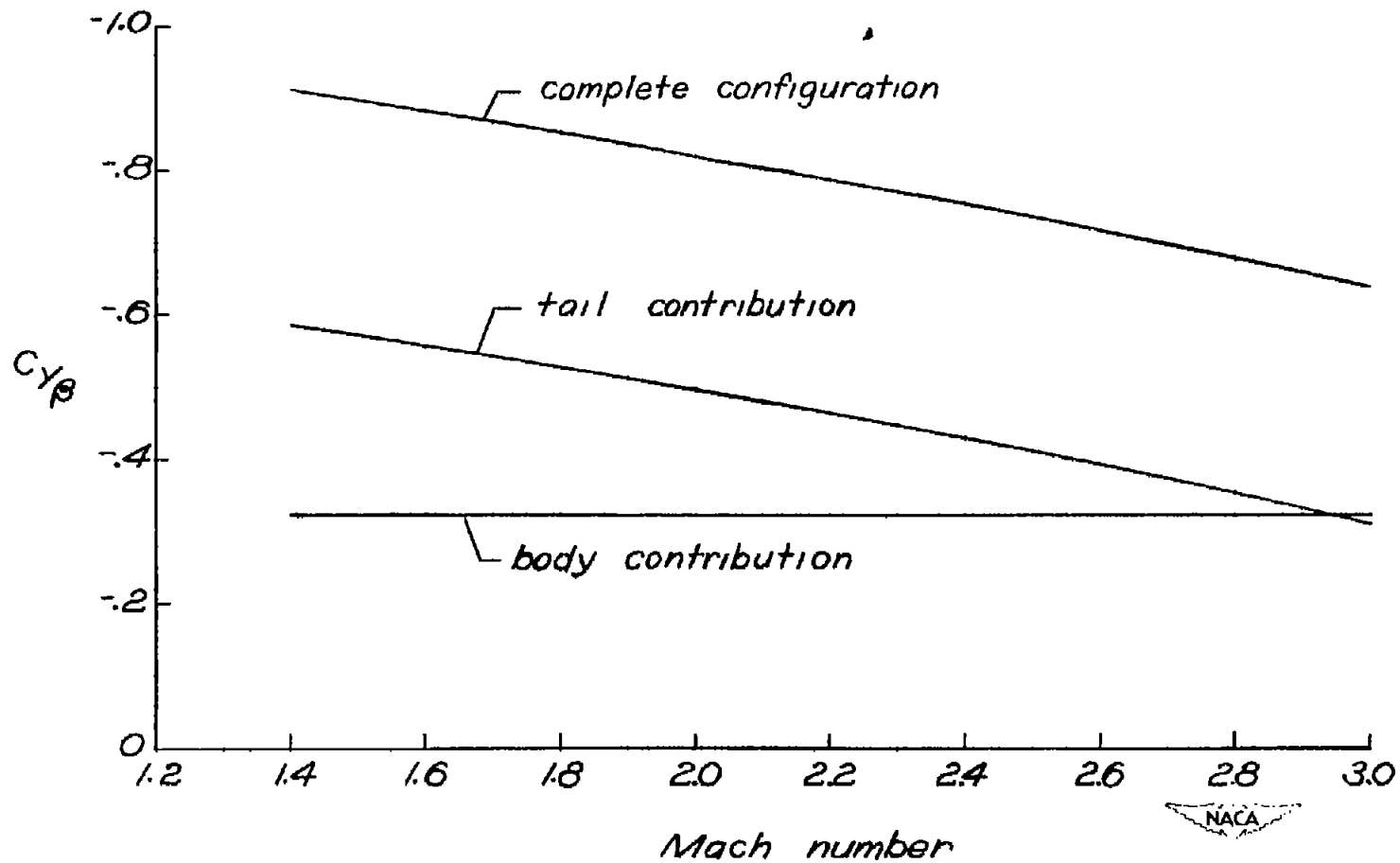


Figure 18.- Variation of the stability derivative $C_{Y\beta}$ with Mach number.

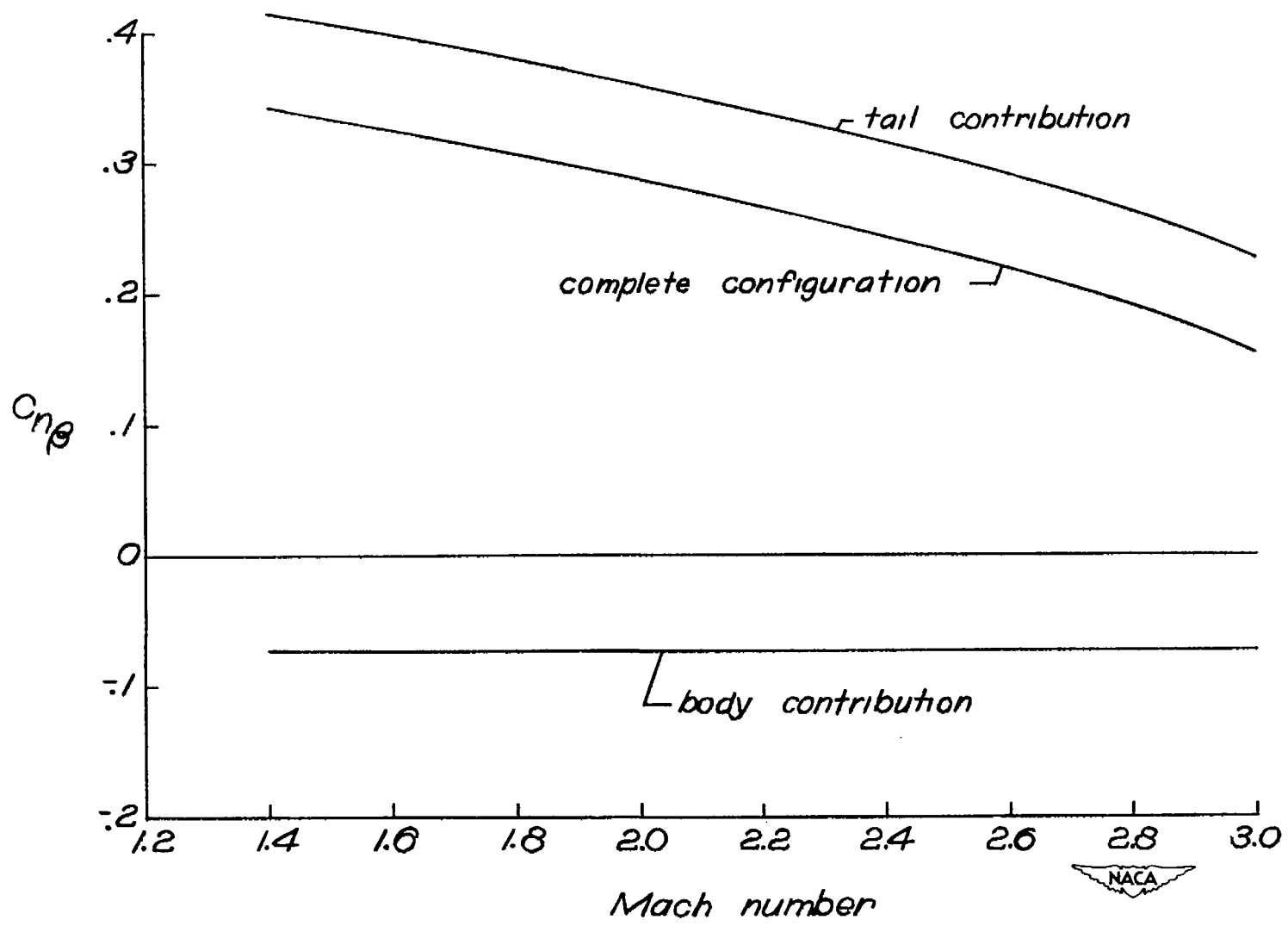


Figure 19.- Variation of the stability derivative $C_{n\beta}$ with Mach number.

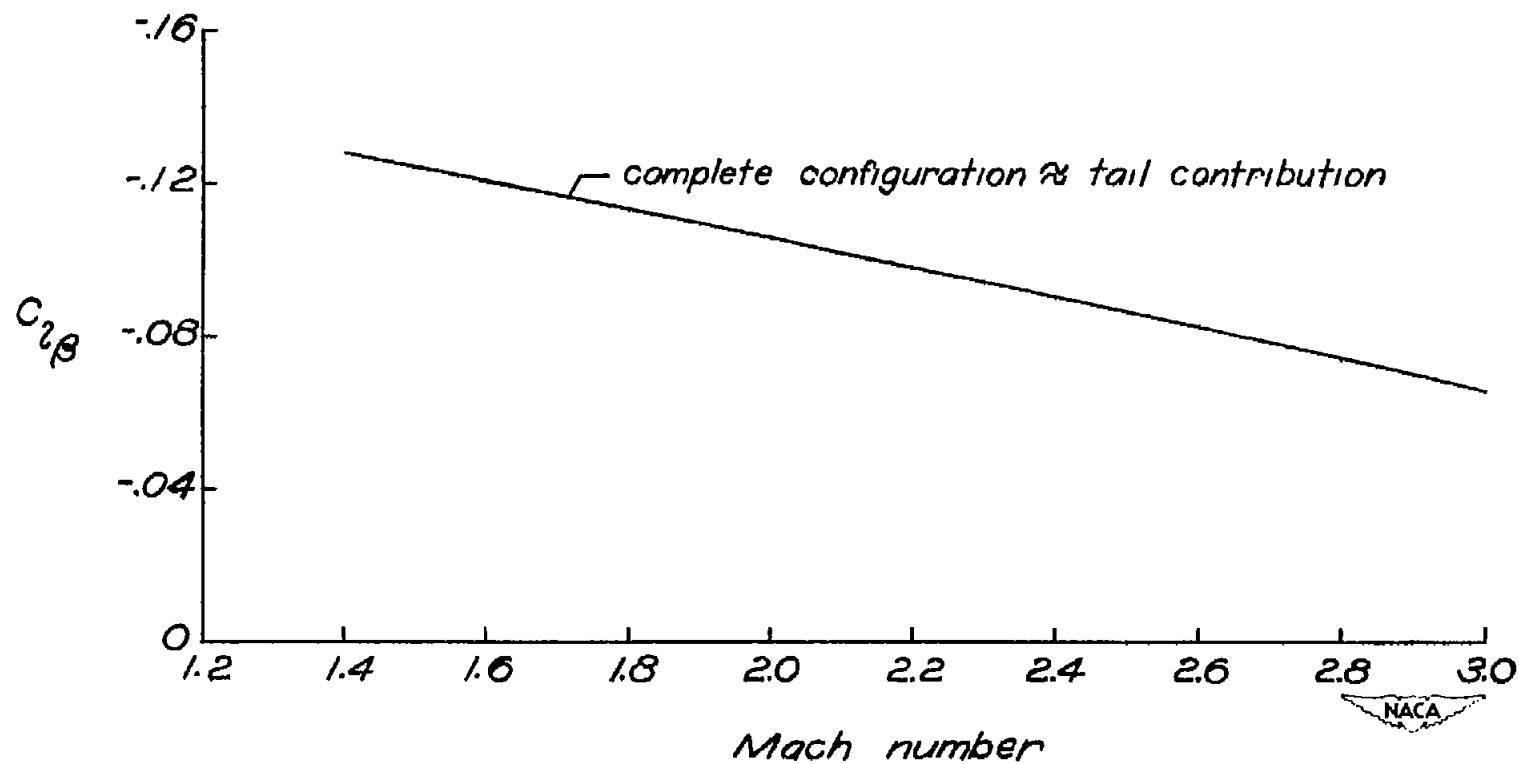


Figure 20.- Variation of the stability derivative $C_{l_{\beta}}$ with Mach number.

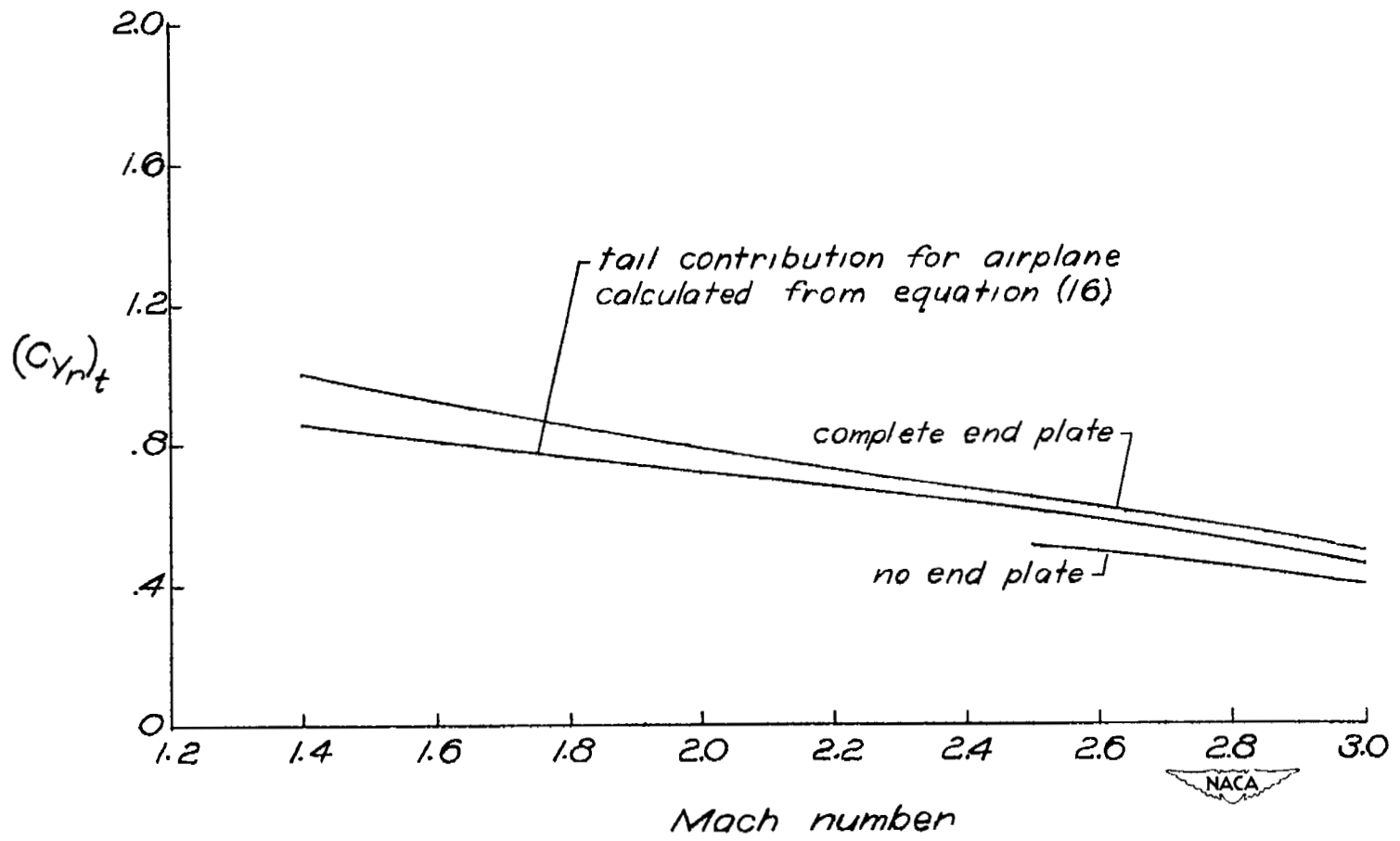


Figure 21.- Comparison of the tail contribution to the stability derivative C_{Yr} calculated from equation (16) with the complete- and no-end-plate solutions.

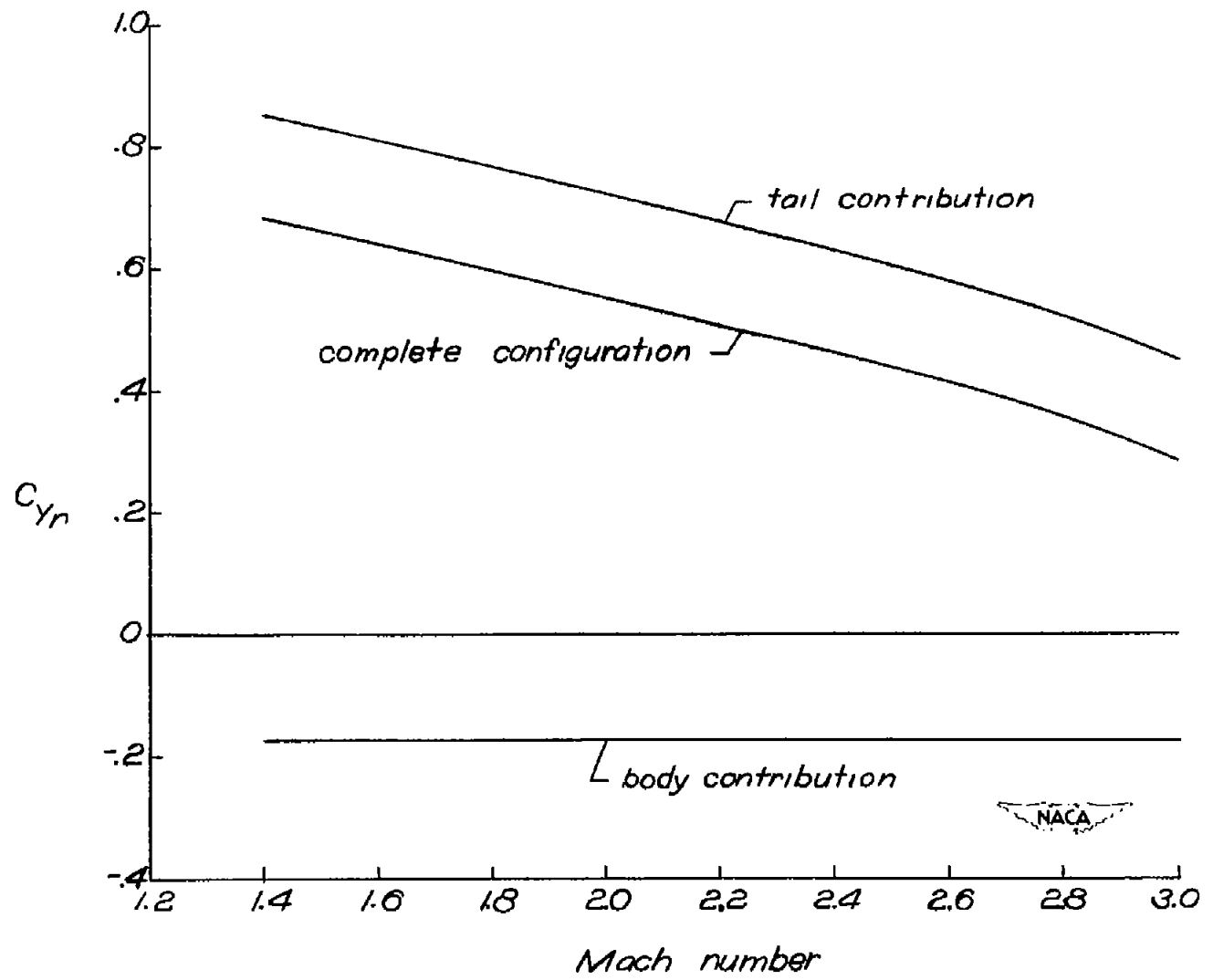


Figure 22.- Variation of the stability derivative C_{Yr} with Mach number.

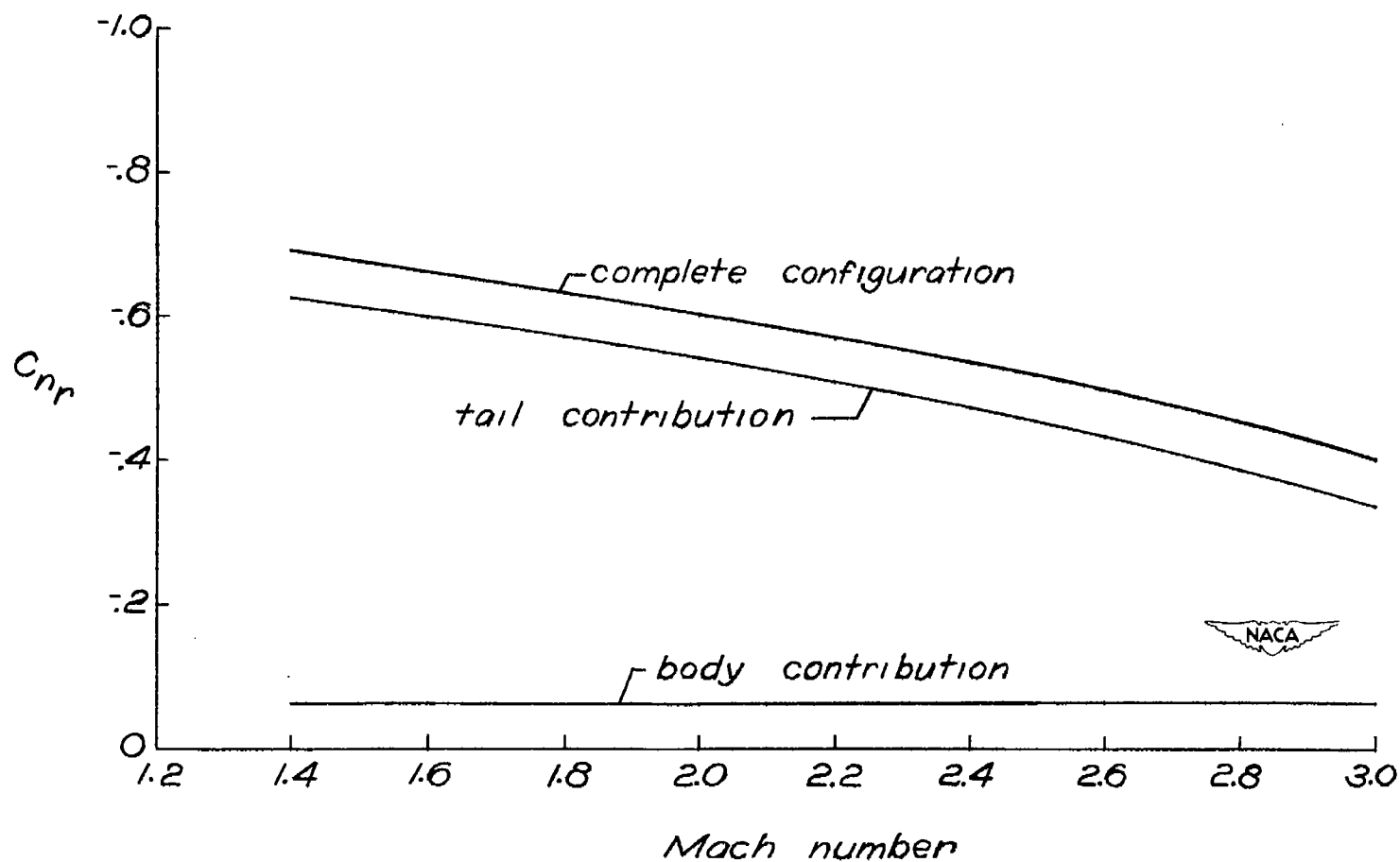


Figure 23.- Variation of the stability derivative C_{nr} with Mach number.

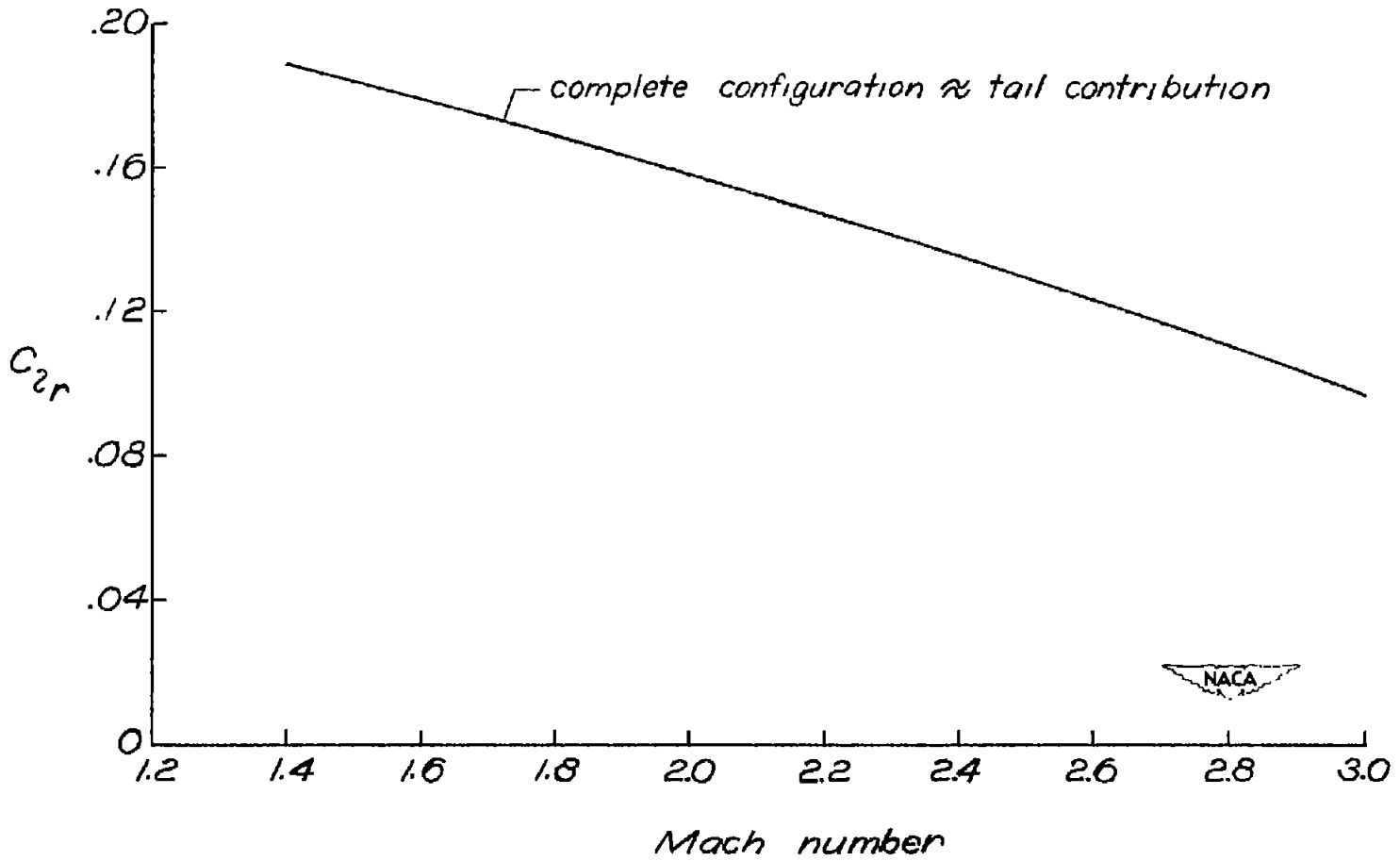


Figure 24.- Variation of the stability derivative C_{Lr} with Mach number.

~~CONFIDENTIAL~~

UNCLASSIFIED



UNCLASSIFIED

~~CONFIDENTIAL~~